Angewandte Chemie
Eine Zeitschrift der Gesellschaft Deutscher Chemiker

Supporting Information

69451 Weinheim, Germany

Chemical and Structural Stability of Zirconium-based Metal–Organic Frameworks with Large Three-Dimensional Pores by Linker Engineering**

*Suresh B. Kalidindi, Sanjit Nayak, Michael E. Briggs, Susanna Jansat, Alexandros P. Katsoulidis, Gary J. Miller, John E. Warren, Dmytro Antypov, Furio Corà, Ben Slater, Mark R. Prestly, Carlos Martí-Gastaldo, and Matthew J. Rosseinsky**

anie_201406501_sm_miscellaneous_information.pdf

Supplementary Information

.

Table of contents:

SI 1. Experimetal methods

a) Starting materials

$ZrCl_4$ (99.99 %) anhydrous and benzoic acid (≥ 99.5 %) were acquired from Sigma Aldrich. $ZrCl_4$ was stored under N_2 in a schlenk tube which was placed in a desiccator. DMF (≥ 99.8 %) and NMP (97 %) solvent were purchased from Fisher Chemical and Sigma Aldrich, respectively. All reagents and solvents were used without any previous purification unless specified.

b) Characterization

Elemental analysis: Carbon, nitrogen and hydrogen contents were determined by microanalytical procedures using a Thermo EA1112 Flash CHNS-O Analyzer. Utilising the Pregl-Dumas method of "flash" combustion, accurately weighed solid or liquid samples encapsulated in Tin, are introduced into a constantly He purged quartz combustion tube, typically at 950 °C and injected with 10 seconds of pure O_2. Under these conditions, Sn rapidly combusts and produces temperatures of up to 1800° C.

Inductively Coupled Plasma – Optical Emission Spectrometry (ICP): Zirconium content in the solution was determined by ICP. Sample measurements were performed utilising a Spectro Ciros ccd ICP-OES radial view instrument. Instrument parameters from optimisation were, Plasma power 1400W with a nebulising flow of 0.85L/min, coolant flow of 11.5 L/min and auxiliary flow of 0.9 L/min. Line selection for each element was Zr 339.198nm and Zr 343.823nm. Typical RSD values were between 1-1.5% indicating a stable plasma with consistent sample injection and aspiration.

Thermogravimetric analysis: Thermo gravimetric analyses were performed in an air atmosphere using TA instrument SDTQ600. A dried crystalline sample was heated at a rate of 10 ºC/min to 800 ºC with air flow of 50 mL/min.

Liquid state Nuclear Magnetic Resonance Spectroscopy. ^{1}H NMR were recorded on Bruker 400 and 500 MHz instruments with chemical shifts reported relative to the deuterated solvent and TMS.

Gas Sorption Measurements: N_2 adsorption – desorption isotherms were measured at 77 K. The measurements carried out on a 3Flex and on a Tristar II porosimeters of Micromeritics. The specific surface area was calculated applying the BET method in the range of relative pressure ($0.01<P/P_0<0.1$) which was selected according to the consistency criteria of Rouquerol.[1] Total pore volume was estimated from adsorbed amount at $P/P_0 = 0.9$. Non local density functional theory (NLDFT), cylindrical model, was applied to obtain the pore size distribution. CO_2, and CH_4 adsorption-desorption isotherms were measured at 273, 283 and 293 K on a 3Flex porosimeter of Micromeritics. Isosteric heat (Qst) of gas adsorption was calculated after fitting the data points to a virial type thermal equation.[2] High pressure adsorption - desorption isotherms with CO_2 and CH_4 were measured for activated **3C** at 293 K by using an Intelligent Gravimetric Analyzer (IGA) from Hiden. Gas adsorption selectivity of activated **3C** from the equimolar mixture CO_2/CH_4 was calculated according to ideal adsorption selectivity theory (IAST).[3]

Scanning electron microscopy (SEM): Images were taken with an Hitachi S-4800 Field Emission SEM

b) Synthesis of btbaH$_4$/4,4',4'',4'''-([1,1'-biphenyl]-3,3',5,5' tetrayltetrakis(ethyne-2,1 diyl))tetrabenzoic acid

Step 1:

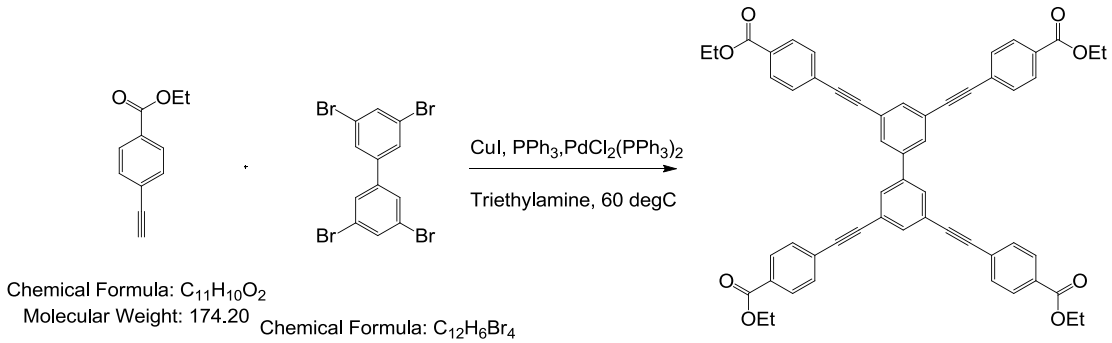

Chemical Formula: $C_{11}H_{10}O_2$
Molecular Weight: 174.20

Chemical Formula: $C_{12}H_6Br_4$
Molecular Weight: 469.79

Chemical Formula: $C_{56}H_{42}O_8$
Molecular Weight: 842.93

Bis(triphenylphosphine)palladium(II) dichloride (0.604 g, 0.86 mmol) was charged to a mixture of 3,3',5,5'-tetrabromo-1,1'-biphenyl (4.0 g, 8.51 mmol), copper iodide (0.320 g, 1.68 mmol), ethyl 4-ethynylbenzoate (8.0 g, 45.9 mmol) and triphenyl phosphine (0.44 g, 1.68 mmol) in triethylamine (200 mL) at 60 °C under a nitrogen atmosphere. After 2 days the mixture was cooled to ambient temperature, water (200 mL) was charged and the precipitate was collected by filtration. The solid was triturated with DCM (500 mL) and filtered to remove any insoluble material. The filtrate was concentrated to a volume of ~40 mL and the suspension was filtered. The crude solid was purified by column chromatography eluting with 0-4 % ethyl acetate/chloroform. The product tetraethyl 4,4',4",4'"-([1,1'-biphenyl]-3,3',5,5'-tetrayltetrakis(ethyne-2,1-diyl))tetrabenzoate containing fractions were concentrated to a volume of ~30 mL, the resulting precipitate was collected by filtration and dried under suction to afford the product as a white solid (2.73 g, 38 %).

^{1}H NMR ($CDCl_3$, 400 MHz): 8.06 (8H, d, *J*=8.6 Hz, Ar-H), 7.80 (4H, s, Ar-H), 7.77 (2H, s, Ar-H), 7.62 (8H, d, *J*=8.6 Hz, Ar-H), 4.40, (8H, q, *J*=7.1 Hz, CH_2), 1.41 (12H, t, *J*=7.1 Hz, CH_3).

Step 2:

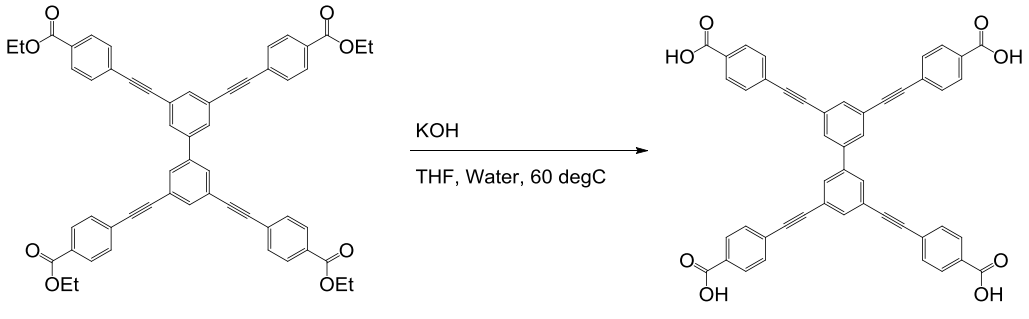

Chemical Formula: $C_{56}H_{42}O_8$
Molecular Weight: 842.93

Chemical Formula: $C_{48}H_{26}O_8$
Molecular Weight: 730.72

Potassium hydroxide (1.40 g, 25.0 mmol) was charged to a suspension of tetraethyl 4,4',4",4'"-([1,1'-biphenyl]-3,3',5,5'-tetrayltetrakis(ethyne-2,1-diyl))tetrabenzoate (2.50 g, 2.97 mmol) in THF (84 mL) and water (28 mL) then the mixture was heated at 60 °C for 3 days.

The reaction was cooled to ambient temperature and the layers were separated. The aqueous layer was diluted with water to a volume of 100 mL then 2M HCl was charged until a pH <2 was obtained. The suspension was filtered and the filter cake was washed with water. The damp filter cake was dried in a vacuum oven at 40 °C for 2 days to afford 1.93 g (85 %, based on $btbaH_4(H_2O)_2$) of material as a white solid.

^{1}H NMR (DMSO-d_6, 400 MHz): 13.22 (4H, br s, CO_2H), 8.15 (4H, d, *J*=1.4 Hz, Ar-H), 8.01 (8H, d, *J*=8.5 Hz, Ar-H), 7.87 (2H, t, *J*=1.4 Hz, Ar-H), 7.74 (8H, d, *J*=8.5 Hz, Ar-H).

EA: $C_{48}H_{26}O_8 \cdot 2H_2O$, Cal.(%): C, 75.19; H, 3.94. Exp.(%): C, 75.11; H, 3.67.

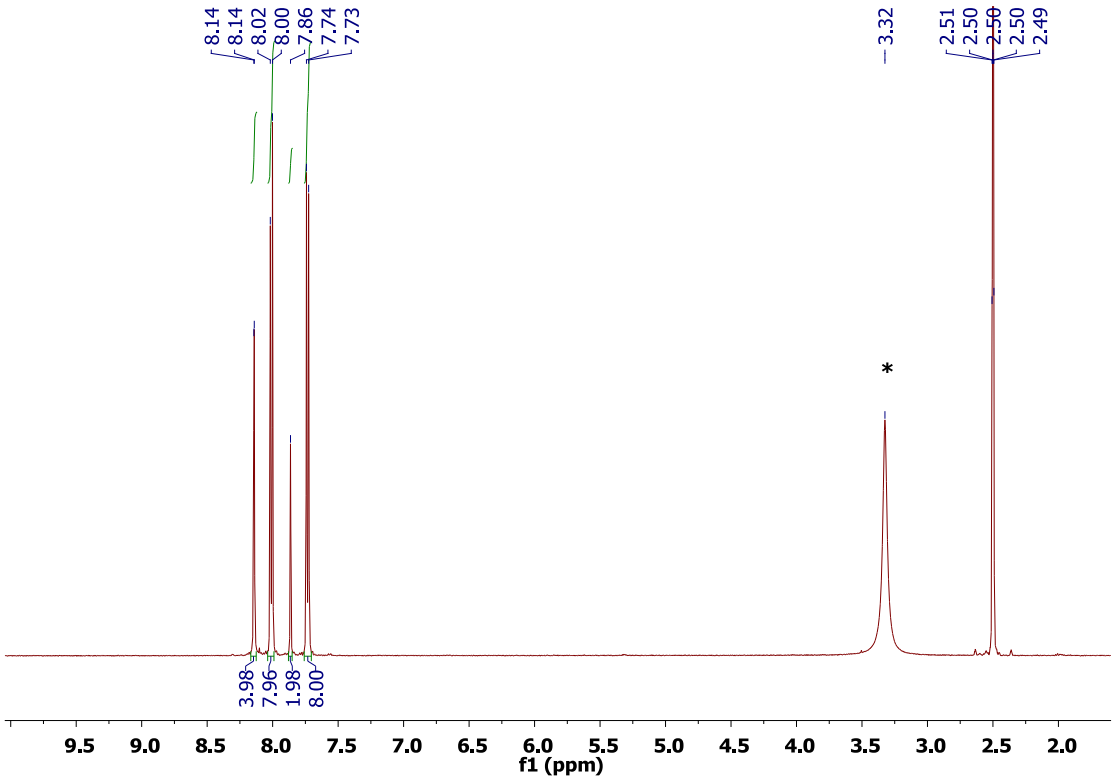

Figure S1: ^{1}H NMR spectrum of $btbaH_4$ ligand in DMSO-d_6 (* from water).

c) Synthesis of ptbaH$_4$/4,4',4'',4'''-(pyrene-1,3,6,8-tetrayltetrakis(ethyne-2,1-diyl))tetrabenzoic acid

Step 1:

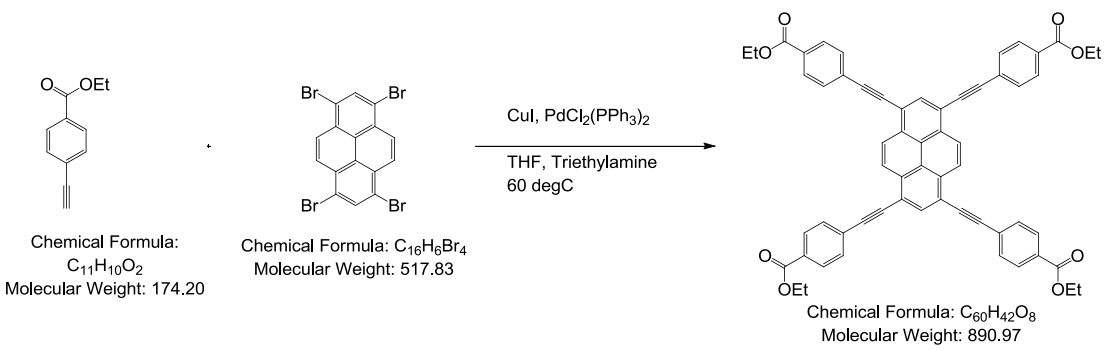

The material was made using a modified literature procedure.[4]A degassed mixture of 1,3,6,8-tetrabromopyrene (3.68 g, 7.1 mmol), CuI (68 mg, 0.357 mmol), ethyl 4-ethynylbenzoate (6.20 g, 35.6 mmol) and bis(triphenylphosphine)palladium(II) dichloride (0.248 g, g, 0.353 mmol) in THF (200 mL) and triethylamine (200 mL) was heated at 60 °C under an argon atmosphere. After 2 days the reaction mixture was cooled to ambient temperature, diluted with water (200 mL) and the precipitate collected by filtration. The filter cake was slurried in refluxing chloroform (800 mL) then filtered to remove insoluble material. The filtrate was concentrated to a volume of ~100 mL, the resulting precipitate was collected by filtration, washed with methanol and dried under suction to afford the product as an orange solid (2.67 g, 42 %). The ^{1}H NMR was consistent with that previously reported.

Step 2:

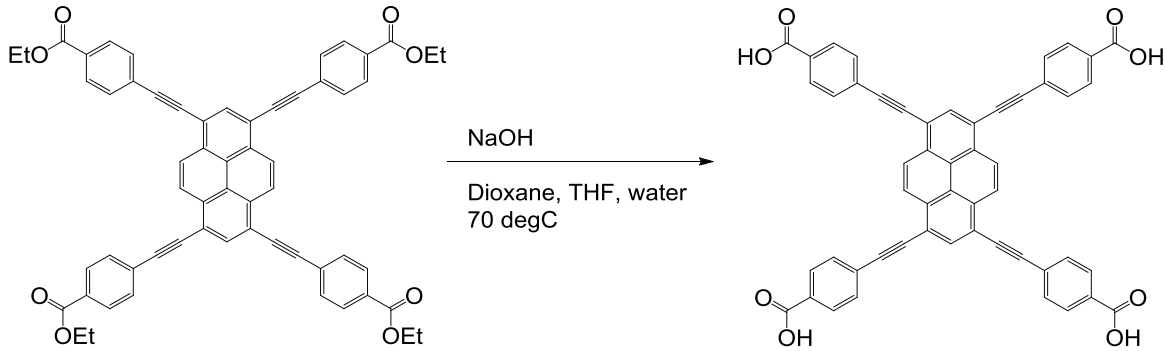

Chemical Formula: $C_{60}H_{42}O_8$
Molecular Weight: 890.97

Chemical Formula: $C_{52}H_{26}O_8$
Molecular Weight: 778.76

Sodium hydroxide (1.96 g, 49.0 mmol) was charged to a suspension of 1,3,6,8-tetrakis[(4-ethoxycarbonylphenyl)ethynyl]pyrene (2.20 g, 2.46 mmol) in THF (140 mL), dioxane (70 mL) and water (70 mL) then the mixture was heated at 70 °C for 2 days. The reaction was cooled to ambient temperature and the reaction mixture was diluted with water (~800 mL) until most of the solid had dissolved. The aqueous mixture was filtered and the filtrate was acidified to pH <3 with 2M HCl. The suspension was filtered and the filter cake was washed with large excess of water. The damp filter cake was dried in a vacuum and recrystallized from DMF at 120 °C to afford bright orange crystals (1.53 g, 75 %) of material.

^{1}H NMR (DMSO-d_6, 400 MHz): 13.12 (4H, br s, CO_2H), 8.40 (4H, br s, Ar-H), 8.27 (2H, br s, Ar-H), 7.95 (8H, d, *J*=8.2 Hz, Ar-H), 7.76 (8H, d, *J*=8.0 Hz, Ar-H).

EA: $C_{52}H_{26}O_8 \cdot 2H_2O(C_3H_7NO)_{0.07}$ Cal. (%): C, 76.48; H, 3.75; N, 0.12; Exp. (%): C, 76.27; H: 3.19; N, 0.11.

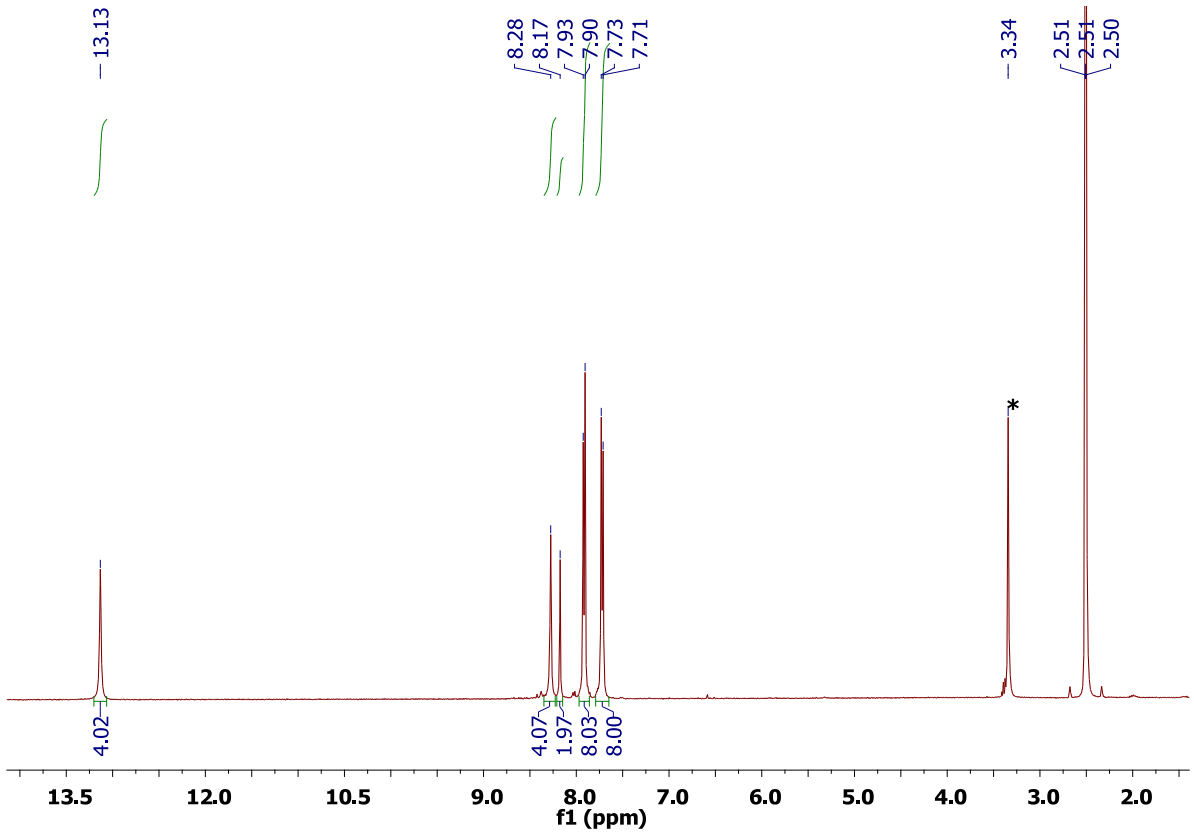

Figure S2: ^{1}H NMR spectrum of $ptbaH_4$ ligand in DMSO-d_6 (* from water).

d) Synthesis of Zrbtba 1

In a 40 mL clear glass Wheaton sample vial with a rubber-lined cap, anhydrous $ZrCl_4$ (0.054 g, 0.23 mmol) and benzoic acid (2.400 g, 19.66 mmol) was dissolved in 12 mL of DMF using ultrasound bath for 30 min at 55 °C. The resulting solution was stored at room temperature for 15 minutes. To this clear solution $btbaH_4$ (0.054 g, 0.070 mmol) was added and the resulting heterogeneous mixture was put in an ultrasound bath at room temperature for another 10 minutes. Finally, the vial was placed into an oven and heated with a ramp rate of 0.2 °C/minute to 120 °C for 96 hours followed by cooling to 25 °C at a rate of 0.5 °C / minute. Shiny cubic crystals of the compound **1** were found at the bottom and the walls of the vial at the end of the reaction. The product was isolated by filtration and cleaned with DMF (3 × 30 mL). Yield: 0.100 g (19 %, based on $btbaH_4$).

CHN data:

As-made MOF, **1**: Formula: $[Zr_6O_4(OH)_4(C_{48}H_{22}O_8)_3](C_7H_6O_2)_{0.18}(C_3H_7NO)_{56}(H_2O)_{23}$; Cal(%): C, 50.92; H, 6.94; N, 10.62; Found: C, 50.90; H, 6.31; N, 10.56.

The as-made material **1** was activated with supercritical CO_2 and exposed to air before analysis. Activated **1**: Formula: $[Zr_6O_4(OH)_4(C_{48}H_{22}O_8)_3](C_7H_6O_2)_{0.18}(H_2O)_5$; Cal.(%): C, 58.71; H, 2.75; Exp.(%): C, 58.23; H, 2.44.

e) Synthesis of Zrptba 2

In a 40 mL clear glass Wheaton sample vial with a rubber lined cap, anhydrous $ZrCl_4$ (0.036 g, 0.15 mmol) and (1.600 g, 13.11 mmol) benzoic acid was dissolved in 8 mL of below given solvent/solvent mixture using an ultrasound bath for 30 minutes at 55 °C. The resulting

solution was stored at room temperature for 30 minutes. To this clear solution 0.028 g (0.034 mmol) of $ptbaH_4$ was added and the resulting heterogeneous mixture was put in an ultrasound bath at room temperature for another 10 minutes. The vial was tightly capped and put into an oven and heated with a ramp rate of 0.2 °C/minute to 120 °C for 72 hours followed by cooling to 25 °C at a rate of 0.5 °C/minute. Shiny orange red crystals of the compound **2** were found at the bottom and the walls of the vial at the end of the reaction. The product was isolated by filtration and cleaned with DMF (3 × 20 mL). Finally, the solid was dried under vacuum. The above reaction was carried out for following different solvent combinations to synthesize high purity **2**.

The above reaction was carried out for the following given solvent/solvent mixtures to synthesize high purity **2**

i) 8 mL of DMF(only); yield: 40 mg; impure from SEM and XRD data (**Figure S4**).

ii) 4 mL of NMP(only); yield:~1 mg; very low yield.

iii) 1 mL of NMP and 7 mL of DMF; yield: 60 mg; impure from SEM and XRD data (**Figure S5**).

iv) 2 mL of NMP and 6 mL of DMF; yield: 50 mg; impure from SEM and XRD data (**Figure S6**).

v) The optimal solvent mixture is 3 mL of NMP and 5 mL of DMF; yield: 55 mg (22% based on $ptbaH_4$).

CHN data for material from reaction condition v:

As-made MOF, **2**: Formula: $[Zr_6O_4(OH)_4(C_{52}H_{22}O_8)_{2.75}(OH)]$ $(C_7H_6O_2)_{0.25}(C_3H_7NO)_{45}(H_2O)_{40}$; Cal(%): C, 48.93; H, 6.78; N, 9.18; Exp(%): C, 48.95; H, 6.23; N, 9.29.

The as-made material **2** was activated at 70 °C under 10^{-7} mbar and exposed to air before analysis. Activated **2**: Formula: $[Zr_6O_4(OH)_4(C_{52}H_{22}O_8)_{2.75}(OH)](C_7H_6O_2)_{0.25}(H_2O)_2$; Cal.(%): C, 60.09; H, 2.47, N, 0.00; Exp.(%): C, 60.46; H, 2.28; N, 0.00.

f) Synthesis of 3A

In a 40 mL clear glass Wheaton sample vial with a rubber lined cap, anhydrous $ZrCl_4$ (0.036 g, 0.15 mmol) and 1.600 g (13.11 mmol) of benzoic acid was dissolved in 8 mL DMF using ultrasound bath for 30 minutes at 55 °C. The resulting solution was stored at room temperature for 30 minutes. To this clear solution a mixture of $btbaH_4$ (0.0265 g, 0.036 mmol) and $ptbaH_4$ (0.001 g, 0.002 mmol), was added and the resulting heterogeneous mixture was sonicated at RT for another 10 minutes. The reaction vial was placed in an oven and heated (0.2 °C / minute) at 120 °C for 72 hours followed by a cooling down to 25 °C at a rate of 0.5 °C /minute. Yellow crystals of the compound **3A** were found at the bottom and walls of the vial at the end of the reaction. The product was isolated by filtration and cleaned with DMF (3 x 20 mL). Finally, the solid was dried under vacuum. Yield: 0.015 g (84 % based on $ptbaH_4$; 6% based on $btbaH_4$).

CHN data:

As-made MOF, **3A**: Formula: $[Zr_6O_4(OH)_4(C_{48}H_{22}O_8)_{2.6}(C_{52}H_{22}O_8)_{0.4}](C_7H_6O_2)_{0.25}$ $(C_3H_7NO)_{48}(H_2O)_{38}$;

Cal(%): C, 49.27; H, 6.86; N, 9.47; Exp(%): C, 49.17; H, 6.07; N, 9.86.

The as-made material **3A** was activated at 70 °C under 10^{-7} mbar and exposed to air before analysis. Activated **3A**: Formula: $[Zr_6O_4(OH)_4(C_{48}H_{22}O_8)_{2.6}(C_{52}H_{22}O_8)_{0.4}](C_7H_6O_2)_{0.25}(H_2O)_4$; Cal.(%): C, 59.36; H, 2.69; Exp.(%): C, 59.18; H, 2.47.

g) Synthesis of 3B

In a 40 mL clear glass Wheaton sample vial with a rubber lined cap, anhydrous $ZrCl_4$ (0.036 g, 0.15 mmol) and 1.6 g (13.11 mmol) of benzoic acid was dissolved in a mixture of 7.5 mL of DMF and 0.5 mL of NMP using an ultrasound bath for 30 minutes at 55 °C. The resulting solution was stored at room temperature for 30 minutes. To this clear solution a mixture of $btbaH_4$ (0.0175 g, 0.023 mmol) and $ptbaH_4$ (0.0090 g, 0.011 mmol), was added and the resulting heterogeneous mixture was sonicated at RT for another 10 minutes. The reaction vial was placed in an oven and heated (0.2 °C/ minute) at 120 °C for 72 hours followed by a cooling down to 25 °C at a rate of 0.5 °C /minute. Yellow orange crystals of the compound **3B** were found at the bottom and wall of the vial at the end of the reaction. The product was isolated by filtration and cleaned with DMF (3 x 20 mL). Finally, the solid was dried under vacuum. Yield: 0.048 g (58 % based on $ptbaH_4$; 29 % based on $btbaH_4$)

CHN data:

As-made MOF, **3B**: Formula:

$[Zr_6O_4(OH)_4(C_{48}H_{22}O_8)_{1.5}(C_{52}H_{22}O_8)_{1.5}](C_7H_6O_2)_{0.45}(C_3H_7NO)_{48}(H_2O)_{46}$;

Cal(%): C, 48.73; H, 6.89; N, 9.18; Exp(%): C, 48.73; H, 5.94; N, 9.46.

The as-made material **3B** was activated at 70 °C under 10^{-7} mbar and exposed to air before analysis. Activated **3B**: Formula:$[Zr_6O_4(OH)_4(C_{48}H_{22}O_8)_{1.5}(C_{52}H_{22}O_8)_{1.5}](C_7H_6O_2)_{0.45}(H_2O)_5$; Cal.(%): C, 59.79; H, 2.71; Exp.(%): C, 59.53; H, 2.40.

h) Synthesis of 3C

In a 40 mL clear glass Wheaton sample vial with a rubber lined cap, anhydrous $ZrCl_4$ (0.036 g, 0.15 mmol) and 1.6 g (13.11 mmol) of benzoic acid was dissolved in 8 mL of below given solvent/solvent mixture using an ultrasound bath for 30 minutes at 55 °C. The resulting solution was stored at room temperature for 30 minutes. To this clear solution a mixture of $btbaH_4$ (0.010 g, 0.013 mmol) and $ptbaH_4$ (0.018 g, 0.022 mmol) was added and the resulting heterogeneous mixture was sonicated at RT for another 10 minutes. The reaction vial was placed in an oven and heated (0.2 °C /minute) at 120 °C for 72 hours followed by cooling to 25 °C at a rate of 0.5 °C / minute. Orange crystals of the compound **3C** were found at the bottom and walls of the vial at the end of the reaction. The product was isolated by filtration and cleaned with DMF (3 x 20 mL). Finally, the solid was dried under vacuum.

The above reaction was carried out for the following solvents to synthesize high purity **3C**.

i) 8 mL of DMF (only), yield: 40 mg; impure from SEM and XRD data (**Figure S7**).

ii) The optimal solvent mixture is 2 mL of NMP and 6 mL of DMF; yield: 0.050 g (58 % based on $ptbaH_4$; 29% based on $btbaH_4$).

CHN data for material from reaction condition ii:

As-made MOF, **3C**: Formula:

$[Zr_6O_4(OH)_4(C_{52}H_{22}O_8)_{2.30}(C_{48}H_{22}O_8)_{0.45}(OH)](C_7H_6O_2)_{0.2}(C_3H_7NO)_{44}(H_2O)_{34}$; Cal.(%): C, 49.53; H, 6.70; N, 9.26 Exp.(%): C, 49.26; H, 6.09; N, 9.50.

The as-made material **3C** was activated at 70 °C under 10^{-7} mbar and exposed to air before analysis. Activated **3C**: Formula: $[Zr_6O_4(OH)_4(C_{52}H_{22}O_8)_{2.30}(C_{48}H_{22}O_8)_{0.45}(OH)](C_7H_6O_2)_{0.2}(H_2O)_3$; Cal.(%): C, 59.75; H, 2.52; Exp.(%): C, 59.60; H, 2.29.

SI 2. Pictures of MOF samples

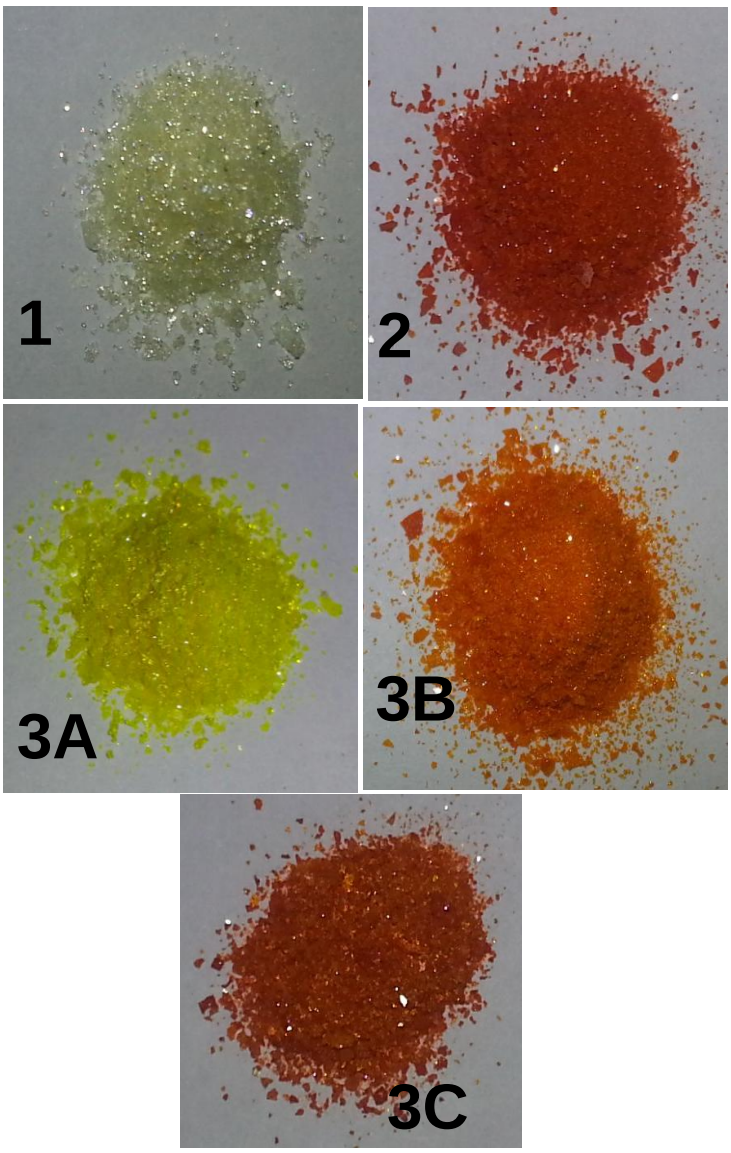

Figure S3: Pictures showing the colours of all MOF samples **(1, 2, 3A, 3B** and **3C).**

SI 3. SEM and XRD data of 2 and 3 for different solvent combinations

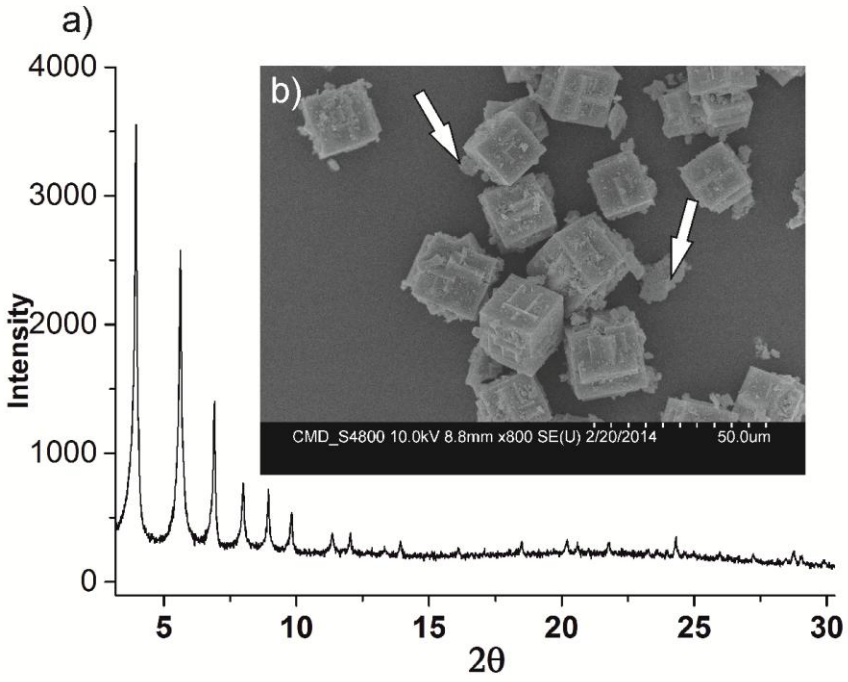

Figure S4: a) PXRD pattern and b) SEM image of **2**, for synthesis in pure DMF. Arrows show the amorphous phase morphology. The amorphous impure phase is present predominantly on the surface of the crystals.

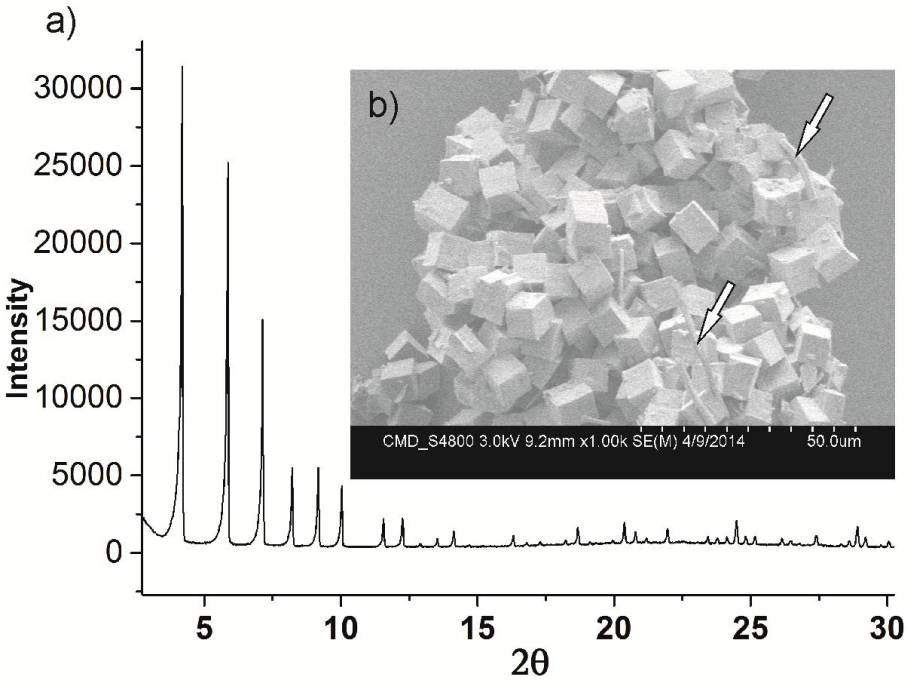

Figure S5: a) PXRD pattern and b) SEM image of **2**, for synthesis with 1 mL of NMP and 7 mL of DMF. Arrows show the belt-like morphology of the impurity.

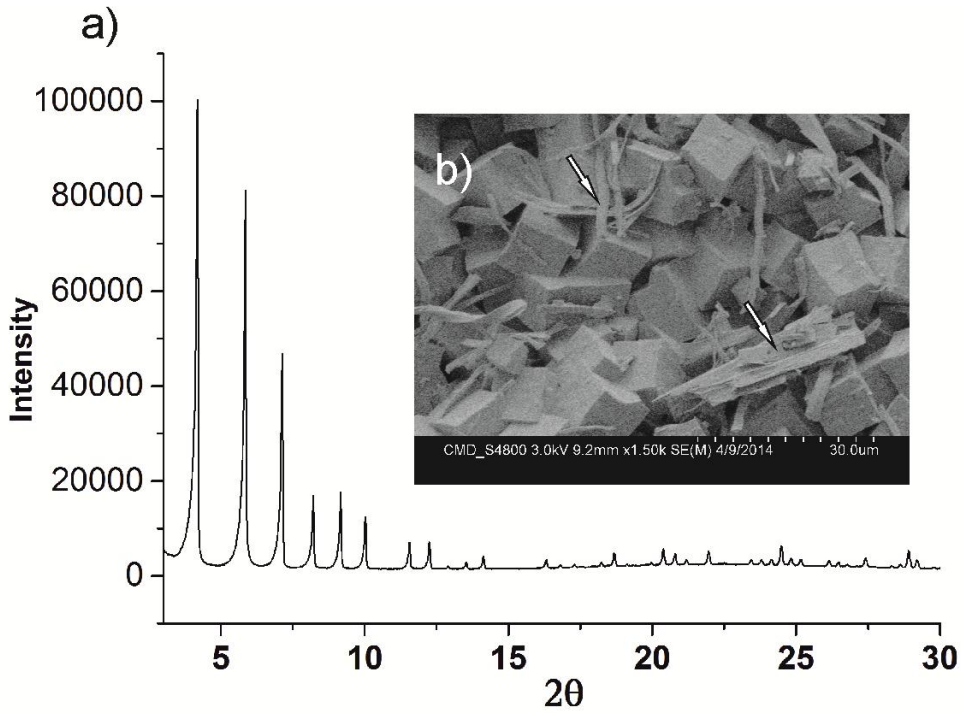

Figure S6: a) PXRD pattern and b) SEM image of **2,** for synthesis with 2 mL of NMP and 7 mL of DMF. Arrows show the belt like morphology of the impurity.

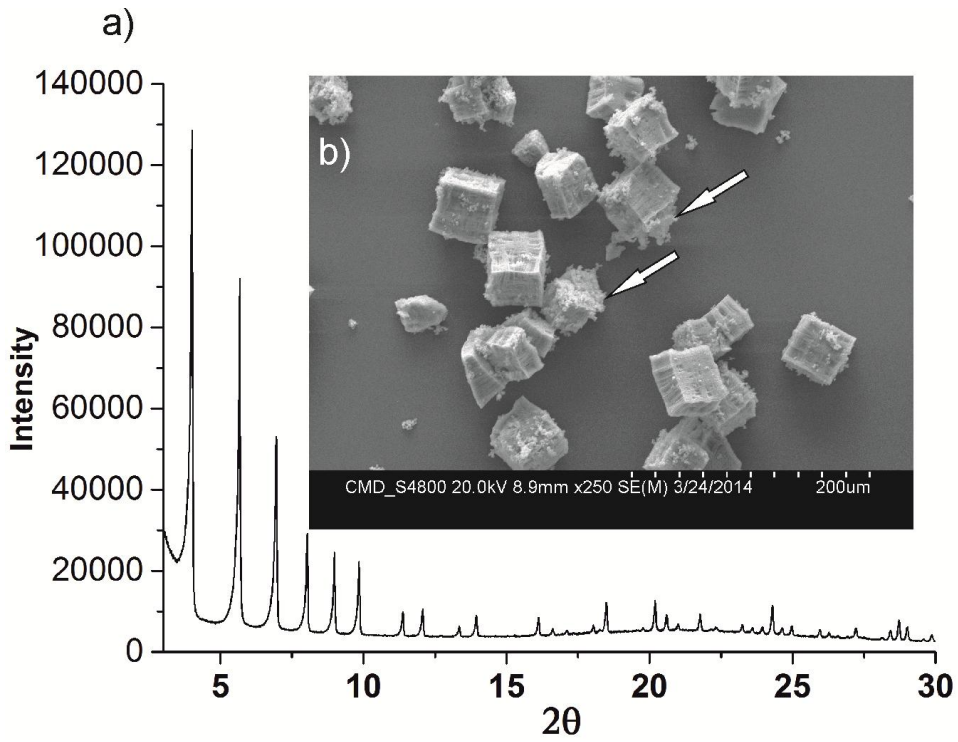

Figure S7: a) PXRD pattern and b) SEM image of **3C**, for synthesis in pure DMF for only DMF reaction. Arrows show the amorphous phase which occurs predominantly on the surface of the crystals.

SI 4. Determination of $ptbaH_4$/$btbaH_4$ ratio in 3A, 3B and 3C by NMR

Digestion procedure using deuterated solvents before ^{1}H-NMR measurement: A drop of 20 wt % DCl in D_2O was added to ~0.3 mg of as-made MOF in a NMR tube. The NMR tube was sonicated at 55 °C for 30 minutes. To this around 0.6 mL of dmso-d_6 was added and final solution was stored at 60 °C for 20 min. This gave a clear solution which was analyzed by ^{1}H NMR. In some cases further dilution with dmso-d_6 was necessary to get good quality spectrum.

The ratio of the two linkers in the MOF was obtained by comparing signals corresponding to the biphenyl and pyrene cores of $btbaH_4$ and $ptbaH_4$, respectively.

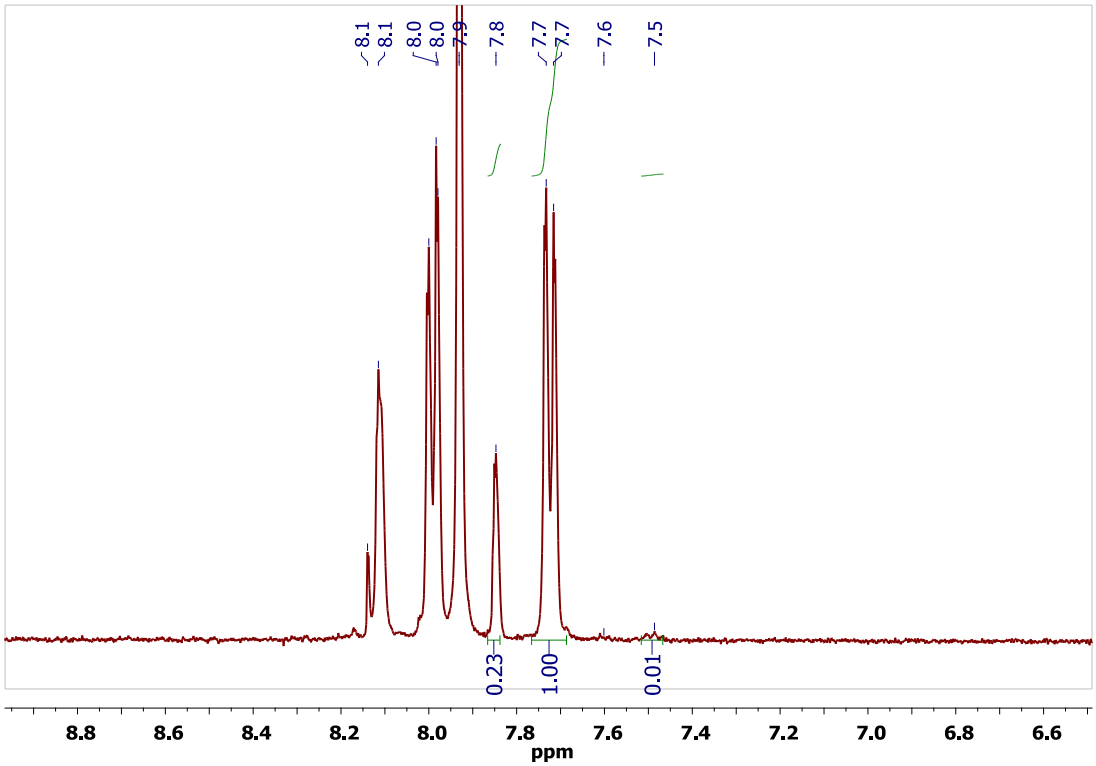

Figure S8. ^{1}H NMR spectrum of **1** in DMSO-d_6 after digestion with 20 wt % DCl. Peaks at 7.5 ppm and 7.6 ppm shows presence of amount of benzoic acid. The ratio of benzoic acid:linker = 0.12:3 was obtained by comparison of peaks at 7.5 ppm (2H, benzoic acid) and 7.7 ppm (8H, $btbaH_4$).

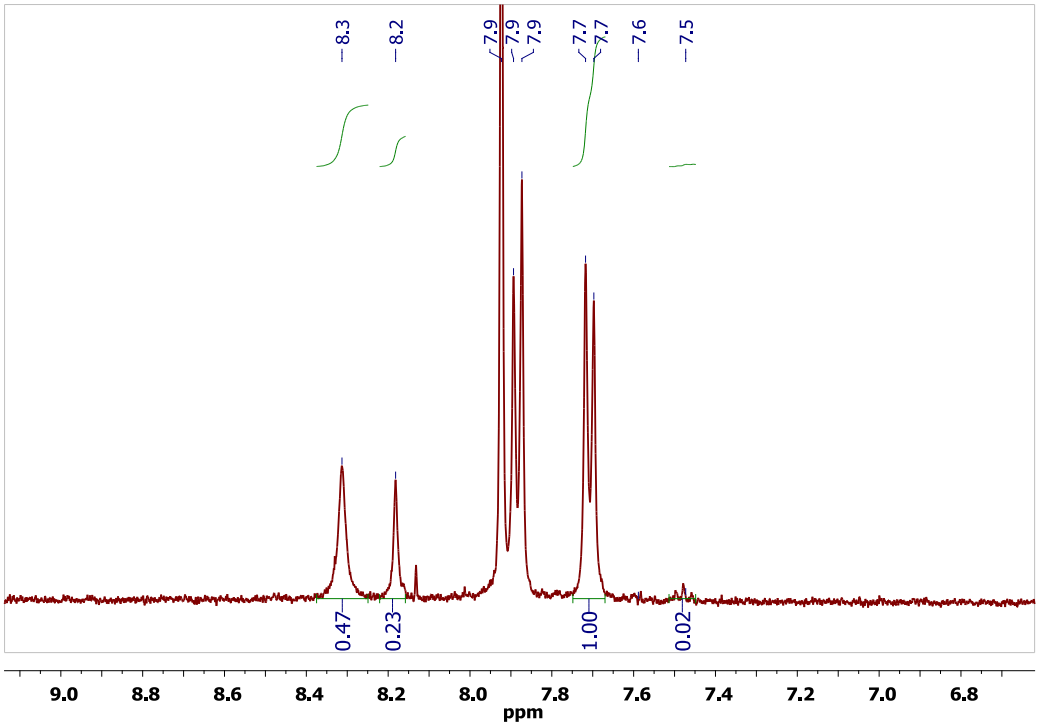

Figure S9. ^{1}H NMR spectrum of **2** in DMSO-d_6 after digestion with 20 wt % DCl. Peaks at 7.5 ppm and 7.6 ppm shows presence of small amount of benzoic acid. The ratio of benzoic acid:linker = 0.21:3 was obtained by comparison of peaks at 7.5 ppm (2H, benzoic acid) and 7.7 ppm (8H, $ptbaH_4$).

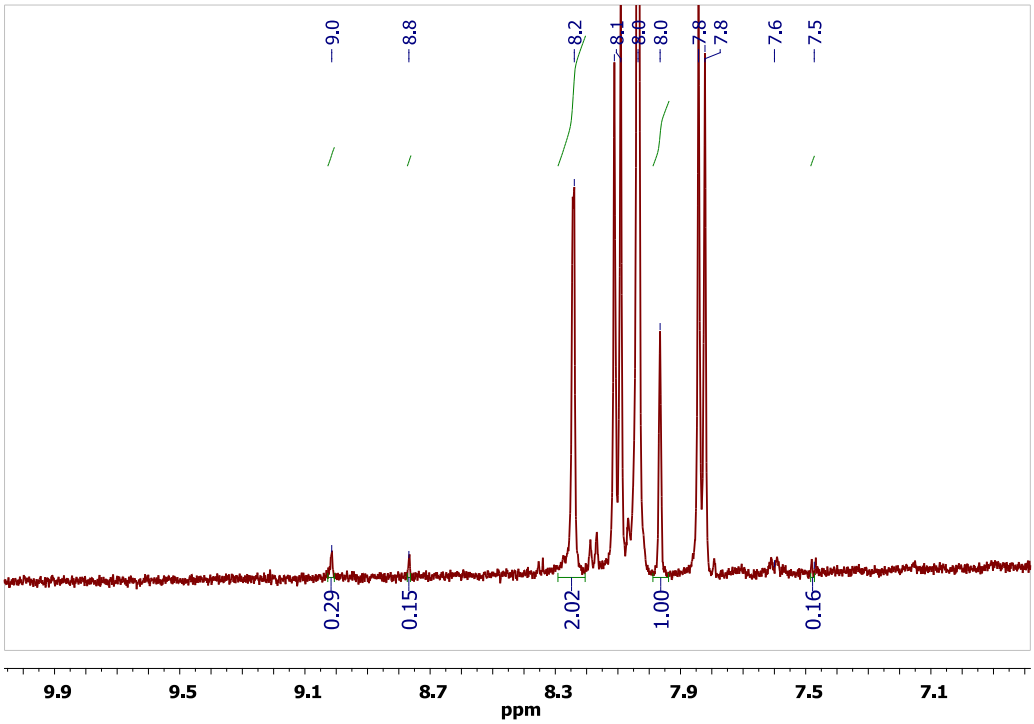

Figure S10. ^{1}H NMR spectrum of **3A** in DMSO-d_6 after digestion with 20 wt % DCl. The ratio of the two linkers in the MOF was obtained by comparison of two different signals of $ptbaH_4$ and $btbaH_4$, 8.8 ppm (2H, $ptbaH_4$) and 8.0 ppm (2H, $btbaH_4$), respectively. Peaks at 7.5 ppm and 7.6 ppm shows presence of small amount of benzoic acid. The ratio of benzoic acid:linker = 0.41:3 was obtained by comparison of peaks at 7.5 ppm (2H, benzoic acid) and 8.0 ppm (2H, $btbaH_4$).

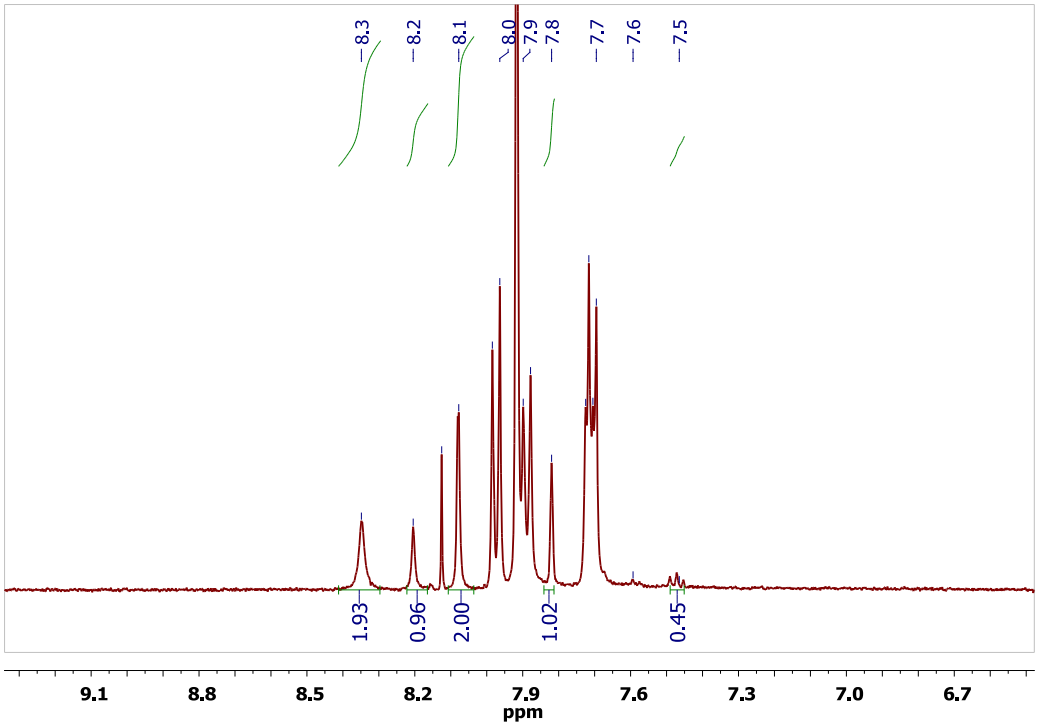

Figure S11. ^{1}H NMR spectrum of **3B** in DMSO-d_6 after digestion with 20 wt % DCl. The ratio of the two linkers in the MOF was obtained by comparison of two different signals of $ptbaH_4$ and $btbaH_4$, 8.2 ppm (2H, $ptbaH_4$) and 7.8 ppm (2H, $btbaH_4$), respectively. Peaks at 7.5 ppm and 7.6 ppm shows presence of small amount of benzoic acid. The ratio of benzoic acid:linker = 0.67:3 was obtained by comparison of peaks at 7.5 ppm (2H, benzoic acid) and 7.8 ppm (2H, $btbaH_4$).

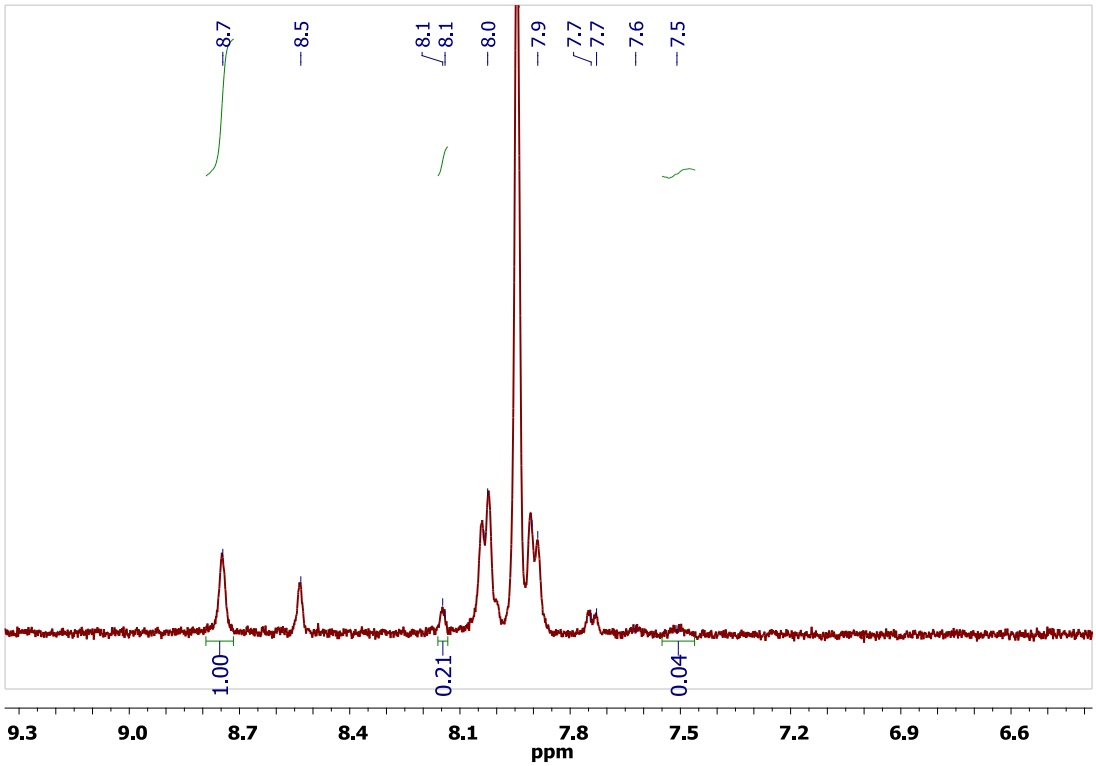

Figure S12. ^{1}H NMR spectrum of **3C** in DMSO-d_6 after digestion with 20 wt % DCl. The ratio of the two linkers in the MOF was obtained by comparison of two different signals of $ptbaH_4$ and $btbaH_4$, 8.7 ppm (4H, $ptbaH_4$) and 8.14 ppm (4H, $btbaH_4$), respectively. Peaks at 7.5 ppm and 7.6 ppm shows

presence of small amount of benzoic acid. The ratio of benzoic acid:linker = 0.22:3 was obtained by comparison of peaks at 7.5 ppm (2H, benzoic acid) and 7.8 ppm (4H, $ptbaH_4$).

SI 5. Activation of MOFs

a) Activation procedure for 1

Initially, as-made **1** was soaked in absolute ethanol, replacing the soaking solution every 8 hours. After the 24 hours exchange process, the ethanol-containing MOF was placed inside a supercritical CO_2 dryer.[5] The ethanol was exchanged with liquid CO_2 over a period of 3 hours, during this time the liquid CO_2 was vented under positive pressure for five minutes every 30 minutes. After that, all the valves are closed and the temperature of the chamber was raised to 40 ºC to reach the critical point of CO_2. The chamber was held in these conditions for an hour and vented slowly over 2 hours. The dried sample was tested for N_2 adsorption immediately.

b) Activation procedure of 2, 3A, 3B, and 3C

The as-made sample was evacuated (10^{-6} mbar) at room temperature for 12 hours. Later, the temperature of the sample was raised to 70 °C and the activation was continued at this temperature for another 12 hours. The final vacuum was 5×10^{-7} mbar. The dried sample was tested for gas adsorption immediately.

SI 6. Thermogravimetric analysis of as-made and activated MOFs

a) Assignment of weight loses

The weight losses in TGA the profiles are assigned based on following protocol. This allowed us to quantify each species accurately.

1) Up to 150 °C: desorption of re-adsorbed water

2) From 150 °C to 330 °C: two events (eq i and ii), decomposition of benzoic acid/benzoate and dehydroxylation of the Zr_6 cluster

$$2C_7H_6O_2(s) + 15O_2\,(g) \longrightarrow 14CO_2\,(g) + 6H_2O\,(g) \quad \text{.... eq (i)}$$

$$Zr_6O_4(OH)_4L_x \longrightarrow Zr_6O_6L_x + 2H_2O \quad L = \text{ptba/btba, } x = 3, 2.75 \quad \text{..eq (ii)}$$

Dehydoxylation of $Zr_6O_4(OH)_4$ cluster (eq ii) to Zr_6O_6 is well established in literature between 250 °C to 300 °C.[6]

To confirm the decomposition of benzoic acid/benzoate takes place below 330 °C, we ran a TGA experiment up to this temperature and analyzed the material for the presence of benzoic acid. The NMR of the material after digestion in DCl/dmso mixture showed no signs of benzoic acid (**Figure S13**), in contrast to the materials activated at lower temperature.

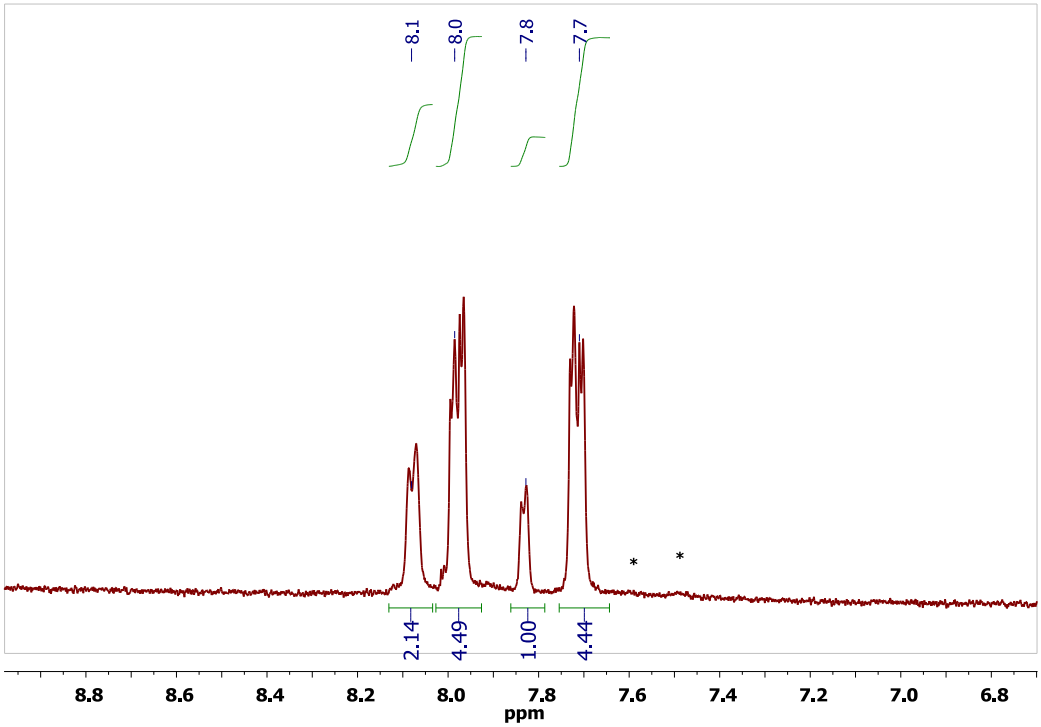

Figure S13: ^{1}H NMR spectrum of **1** after running TGA experiment up to 330 °C and digestion in DCl and dmso mixture. '*' positions where peaks for benzoic acid are expected.

b) TGA profiles of as-made and activated MOFs

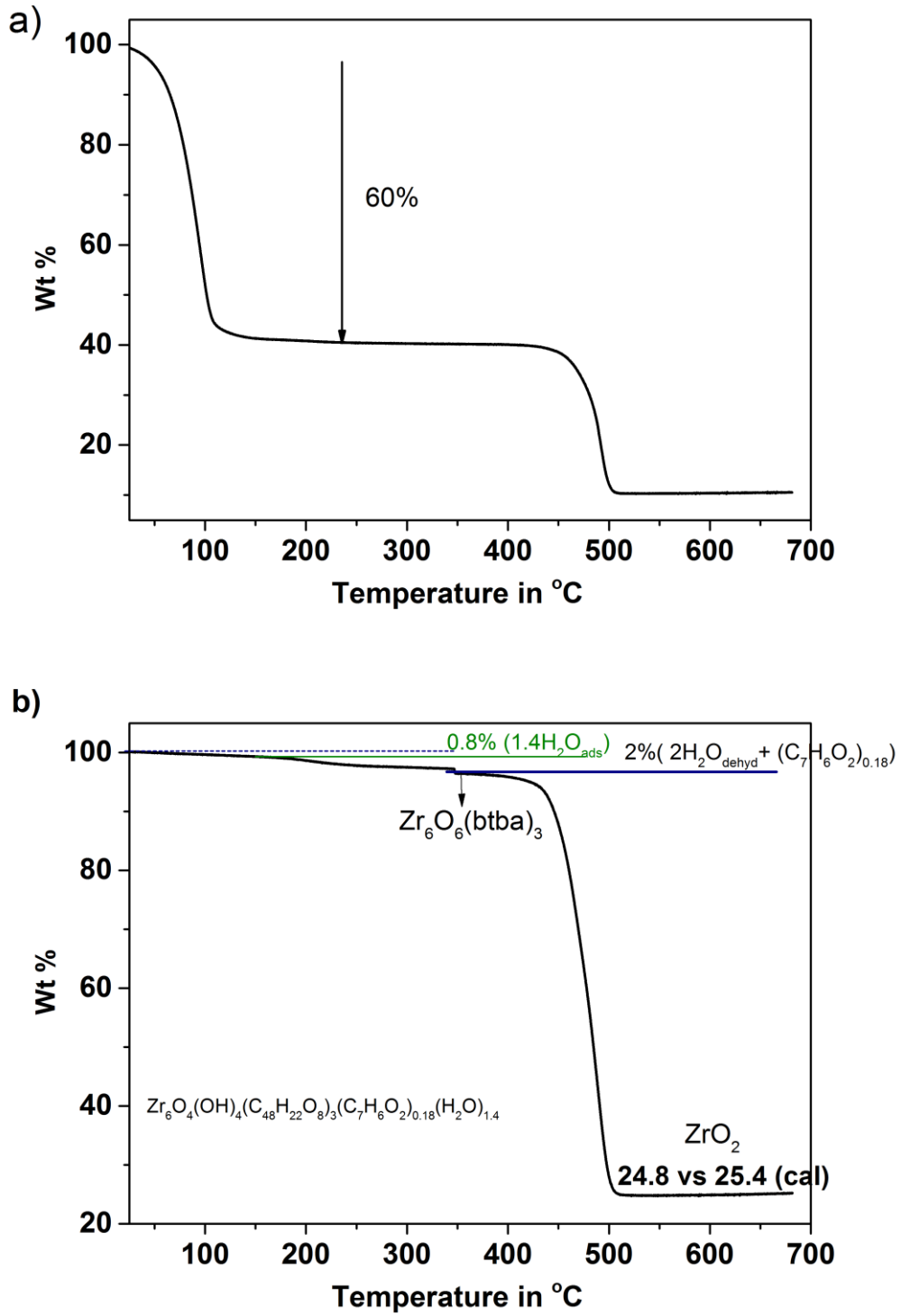

Figure S14: a) TGA profile of as-made **1**; The initial 60 % weight loss below 110 °C is consistent with guest solvent content of 56 molecules of DMF and 23 molecules of water per unit formula derived from CHN data. b) TGA profile of activated **1**; The final ZrO_2 content of activated **1** is consistent with formation of stoichiometric MOF with Zr/linker ratio of 2. The species corresponding to each weight loss and overall formula of MOF obatined from all the assignments is shown in the figure. The formulas obtained from TGA and CHN analysis (section S1d) differ (3.6 molecules) in terms of number of re-adsorbed water molecules.

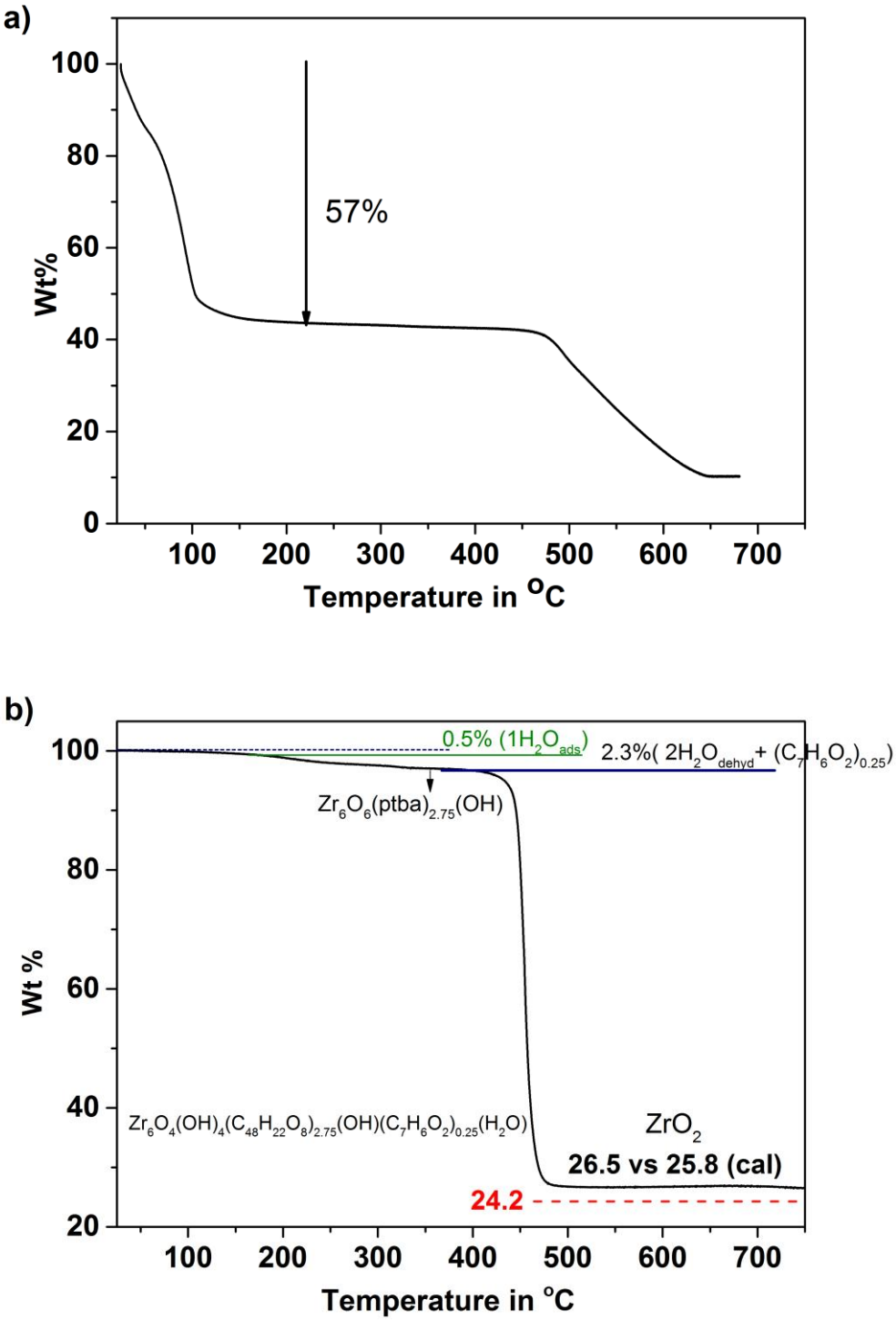

Figure S15: a) TGA profile of as-made **2**; The initial 57 % weight loss below 110 °C is consistent with guest solvent content of 45 molecules of DMF and 40 molecules of water per unit formula derived from CHN data. b) TGA profile of activated **2**; The dotted line (red) shows the final ZrO_2 mass (**Table S1**) expected for the stoichiometric MOF with Zr/linker ratio of 2. The difference of 2.3 % between calculated (for stoichiometric MOF) and observed residual ZrO_2 confirms the presence of ≈ 8 % missing linker defects in **2** and is consitent with the fromula shown in the figure. The species corresponding to each weight loss is also shown. The formulas obtained from TGA and CHN analysis (section S1e) differ (one molecule) in terms of number of re-adsorbed water molecules.

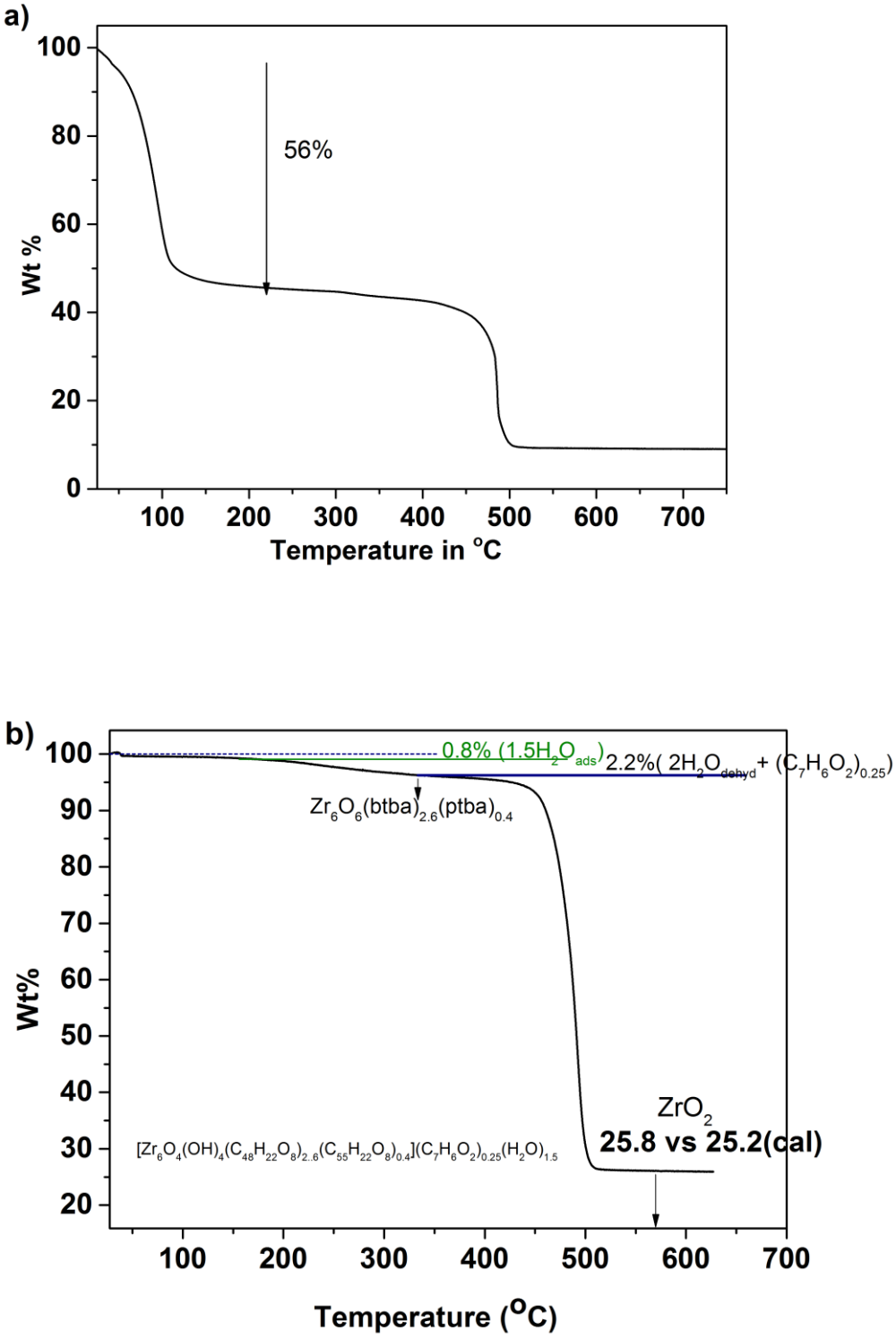

Figure S16: a) TGA profile of as-made **3A**; the initial 55 % weight loss below 110 °C is consistent with guest solvent content of 48 molecules of DMF and 38 molecules of water per unit formula derived from CHN data. b) TGA profile of activated **3A**; The final ZrO_2 content of activated **3A** is consistent with formation of stoichiometric MOF with Zr/linker ratio of 2. The species corresponding to each weight loss and overall composition of MOF obatined from all the assignments is shown in the figure. The formulas obtained from TGA and CHN analysis (section S1f) differ (2.5 molecules) in terms of number of re-adsorbed water molecules.

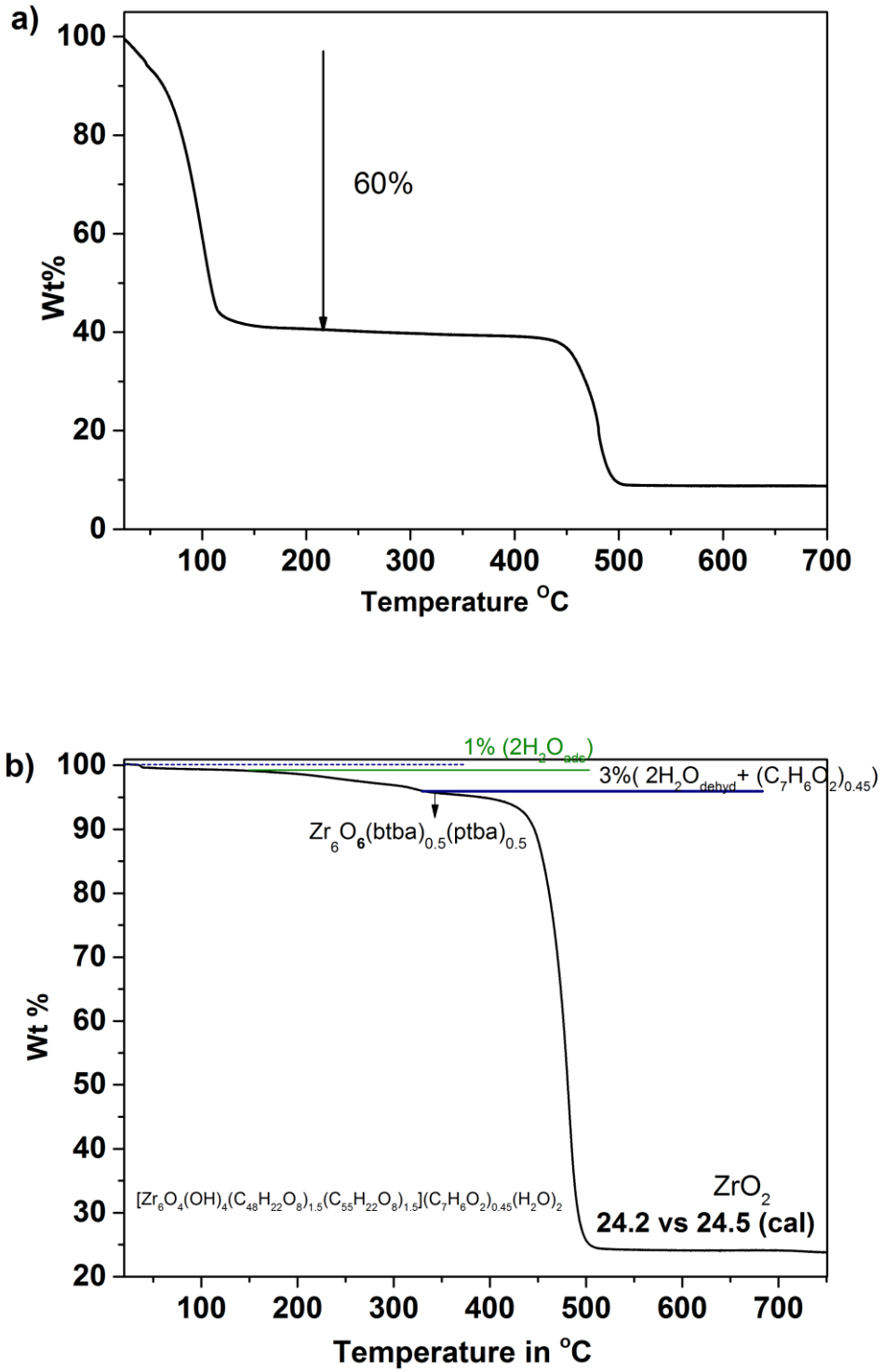

Figure S17: a) TGA profile of as-made **3B**; the initial 60 % weight loss below 110 °C is consistent with guest solvent content of 48 molecules of DMF and 46 molecules of water per unit formula derived from CHN data. b) TGA profile of activated **3B**; The final ZrO_2 content of activated **3B** is consistent with formation of stoichiometric MOF with Zr/linker ratio of 2. The species corresponding to each weight loss and overall composition of MOF obatined from all the assignments is shown in the figure. The formulas obtained from TGA and CHN analysis (section S1g) differ (3 molecules) in terms of number of re-adsorbed water molecules.

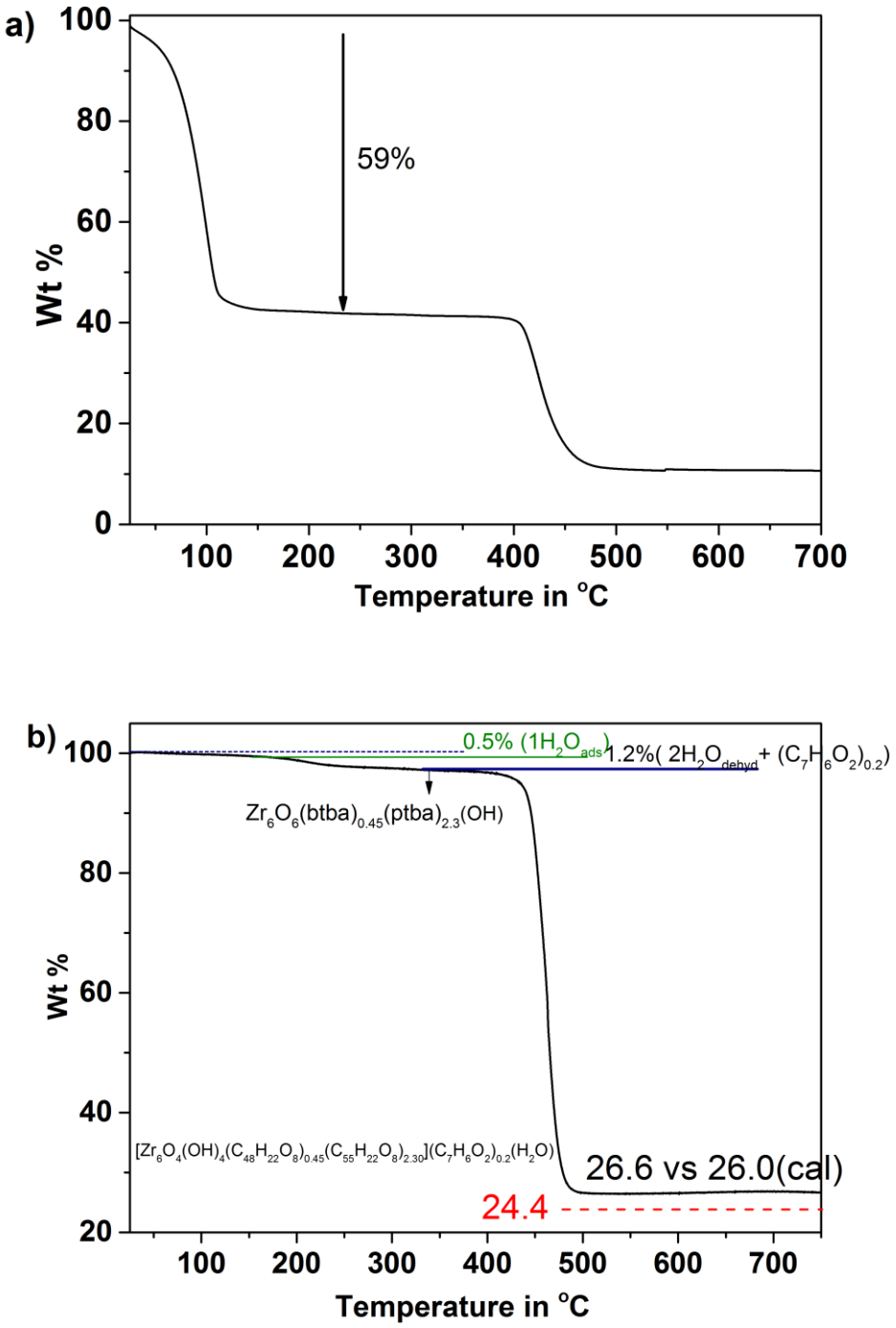

Figure S18: a) TGA profile of as-made **3C**; **t**he initial 59 % weight loss below 110 °C is consistent with guest solvent content of 44 molecules of DMF and 34 molecules of water per unit formula derived from CHN data. b) TGA profile of activated **3C**; The dotted line (red) shows the final ZrO_2 mass expected (**Table S1**) for the stoichiometric MOF with Zr/linker ratio of 2. The difference of 2.3 % between calculated (for stoichiometric MOF) and observed residual ZrO_2 confirms the presence of ≈ 8 % missing linker defects in **3C** and is consitent with the fromula shown in the figure. The species corresponding to each weight loss is also shown. The formulas obtained from TGA and CHN analysis (section S1h) differ (2 molecules) in terms of number of re-adsorbed water molecules.

Table S1. Final ZrO_2 content (calculated/observed) of all MOF samples. All the observed mass losses based on the literature protocol of forming Zr_6O_6 agree within 0.7% at worst, whereas the assumption of full linker stoichiometry leads to disagreement of over 2%.

MOF	Formula (at 330 °C)	Calculated ZrO2%	Observed ZrO2%
1	Zr_6O_6 $(C_{48}H_{22}O_8)_3$	25.4	24.8
2	$Zr_6O_5(C_{52}H_{22}O_8)_{2.75}(OH)$	25.8	26.5
	$Zr_6O_6(C_{52}H_{22}O_8)_3$	24.2	26.5
3A	$Zr_6O_6(C_{48}H_{22}O_8)_{2.6}(C_{52}H_{22}O_8)_{0.4}$	25.2	25.8
3B	$Zr_6O_6(C_{48}H_{22}O_8)_{1.5}(C_{52}H_{22}O_8)_{1.5}$	24.5	24.2
3C	$Zr_6O_6(C_{48}H_{22}O_8)_{0.45}(C_{52}H_{22}O_8)_{2.3}$	26.0	26.6
	$Zr_6O_6(C_{48}H_{22}O_8)_{0.5}(C_{52}H_{22}O_8)_3$	24.4	26.6

The formulas obtained from TGA (shown in **Figures S14-18**) and CHN analysis (SI section **S1d-h**) differ (up to 3 molecules) in terms of number of re-adsorbed water molecules. The number of re-adsorbed water can vary widely depending on the amount of time each sample exposed to air before each measurement, especially in MOFs with large pores such as ours, and partly due to the escape of water molecules during the stabilization of weight under oxygen flow at the initial stage of TGA measurement.

c) Estimation of benzoic acid from NMR and TGA

The peaks from benzoic acid are very weak in ^{1}H NMR (**Figure S8-12**), only just above base line in some cases. However, integration of these peaks show that the values fall well within the range of the linker:benzoic acid ratio obtained from TGA. At the analytical levels at which we detect the benzoic acid, it is not possible to distinguish this from coordination as benzoate to the cluster.

We also looked at the possibility of benzoate occupying the missing linker sites, however, the observed benzoic acid:linker: ratio (0.25:3) suggest that this may not be the case, we need close to 1:3 ratio for complete occupancy of missing linker sites with benzoic acid. Co-ordination of water molecules at missing linker site cannot balance the charge. In this scenario, the most likely possibility is hydroxide ion. Therefore, we arrived to a formula of $[Zr_6O_4(OH)_4(C_{52}H_{22}O_8)_{2.75}(OH)](C_7H_6O_2)_{0.25}(H_2O)$ for **2** and $[Zr_6O_4(OH)_4$ $Zr_6O_6(C_{48}H_{22}O_8)_{0.45}(C_{52}H_{22}O_8)_{2.35}(OH)](C_7H_6O_2)_{0.25}(H_2O)$ for **3C**.

Table S2. Ratios of benzoic acid and linker in each MOF from NMR and TGA

MOF	Benzoic acid:Linker from NMR	Benzoic acid:Linker from TGA
1	0.12:3	0.18:3
2	0.21:3	0.25:3
3A	0.41:3	0.25:3
3B	0.67:3	0.45:3
3C	0.22:3	0.21:3

SI 7. BET Surface areas and pore size distribution of activated MOFs

Table S3: N_2 BET Surface areas of activated MOFs

MOF(activated)	Pore Volume / cm^3g^{-1}		BET surface area/m^2g^{-1}	
	Calculated [a]	Exp. (at $p/p^0 = 0.9$)	Theor.[b]	Exp. (p/p^0=0-0.1)
1 [c]	1.77	1.68	4,460	4,342
2 [d]	1.64	1.55	4,126	4,116
3A [d]	-	1.62	-	4,120
3B [d]	-	1.65	-	4,293
3C [d]	-	1.57	-	4,214

[a] based on solvent accessible volume of single crystal structure, calculated using probe diameter 3.6 Å (equal to kinetic diameter of N_2); [b] Values calculated with Accessible Surface Area Code ©.[7]; [c]. Activation using supercritical CO_2 [d]. Activation at 70 °C, 10^{-7} mbar.

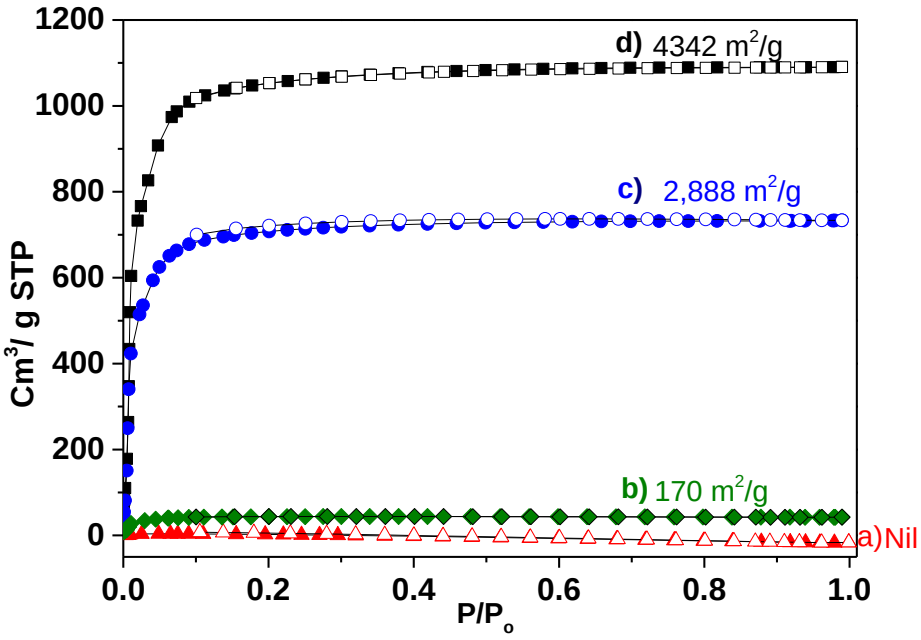

Figure S19. N_2 isotherms of activated **1** at 77 K for different activation procedures: a) activation at RT and 10^{-7} mbar for 1 day; b) Ethanol exchange and activation 10^{-7} mbar at RT for 1 day; c) activation at RT and 10^{-5} mbar for 2 days and d) supercritical CO_2 activation. Filled and empty symbols stand for adsorption and desorption, respectively.

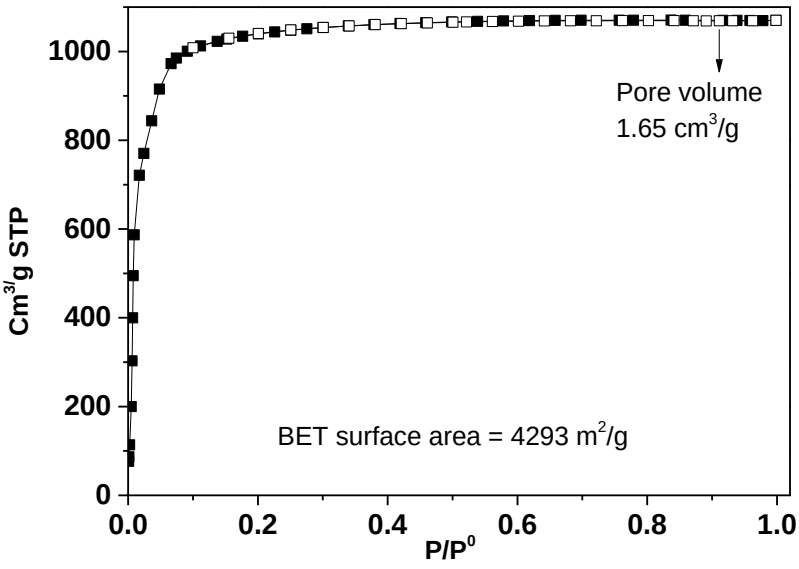

Figure S20. N_2 isotherm of activated **3B** at 77 K. The as-made sample (**3B**) was evacuated (10^{-6} mbar) at room temperature for 12 hours. Later, the temperature was raised to 70 °C and the activation was continued for another 12 hours. Filled and empty symbols stand for adsorption and desorption, respectively.

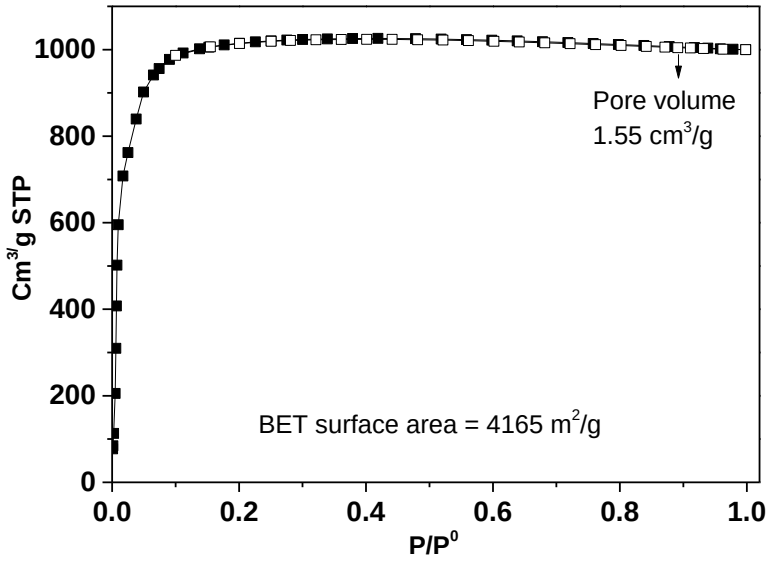

Figure S21. N_2 isotherm of activated **3C** at 77 K. The as-made sample (**3C**) was evacuated (10^{-6} mbar) at room temperature for 12 hours. Later, the temperature was raised to 70 °C and the activation was continued for another 12 hours. Filled and empty symbols stand for adsorption and desorption, respectively.

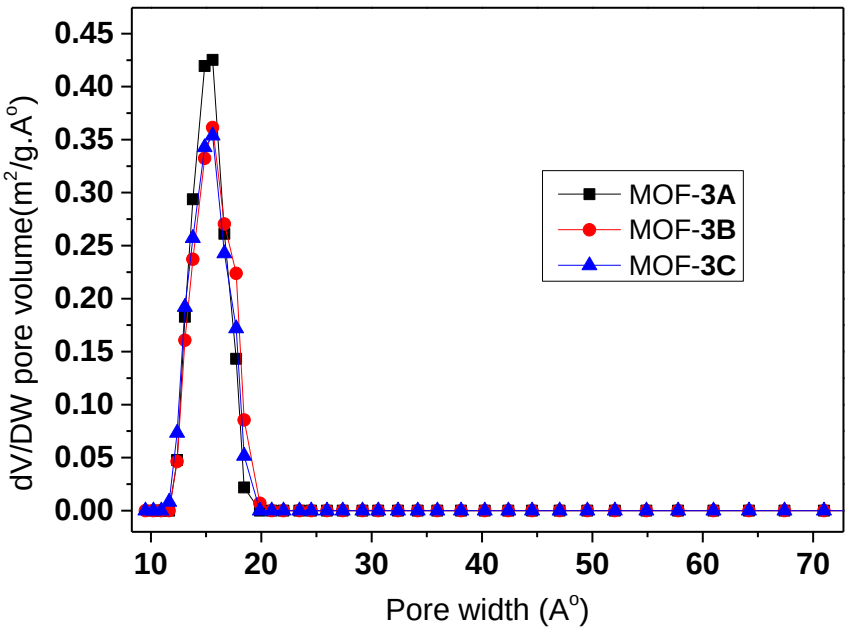

Figure S22. DFT pore size distribution of **3A**, **3B** and **3C**, calculated from N_2 sorption data at 77K. The three materials exhibit very much similar pore size distribution as that of **1** and **2 (**main text, Figure 2d**)**.

SI 8. High-pressure adsorption isotherms of CO_2, CH_4 and N_2

High-pressure adsorption isotherms of CO_2, CH_4 and N_2 on activated **3C** were collected in an Intelligent Gravimetric Analyzer (IGA) at 293 K (**Figure S23**). They exhibit maximum uptakes of 107, 10.5 and 7.6 wt % for CO_2, CH_4 and N_2 at 18.5 bar. The adsorption selectivity from equimolar gas mixtures CO_2:CH_4 and CO_2:N_2 was calculated with the ideal adsorbed solution theory (IAST). The CO_2 adsorption selectivity over CH_4 is 3 from 0 to 10 bars and ranges from 7 to 8 over N_2 for the same pressure range (**Figure S24**). **Figure S27** displays the coverage dependent isosteric heats of CO_2 and CH_4 adsorption (*Qst*) calculated from volumetric adsorption isotherms from 0 to 1 bar at 273, 283 and 293 K. *Qst's* at zero coverage are 12 (CO_2) and 13(CH_4) kJmol^{-1}, suggesting very weak interaction of the adsorbates with the framework, consistent with the large size of the pores.

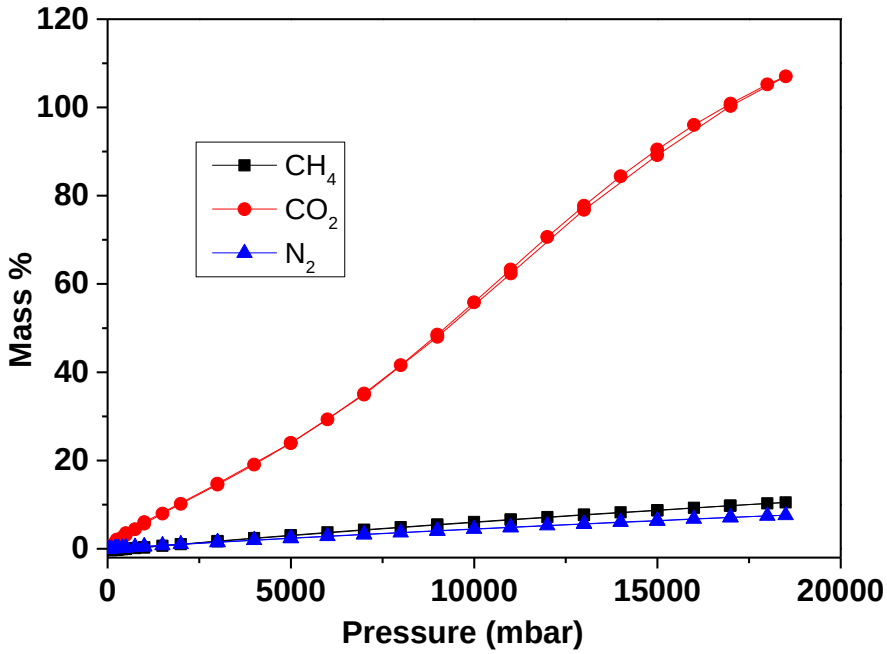

Figure S23. High pressure adsorption isotherms of CO_2, CH_4 and N_2 on activated **3C** using Intelligent Gravimetric Analyzer (IGA) at 293 K. The as-made sample (**3C**) was activated before measurements at 70 °C under 10^{-7} mbar; Filled and empty symbols stand for adsorption and desorption, respectively.

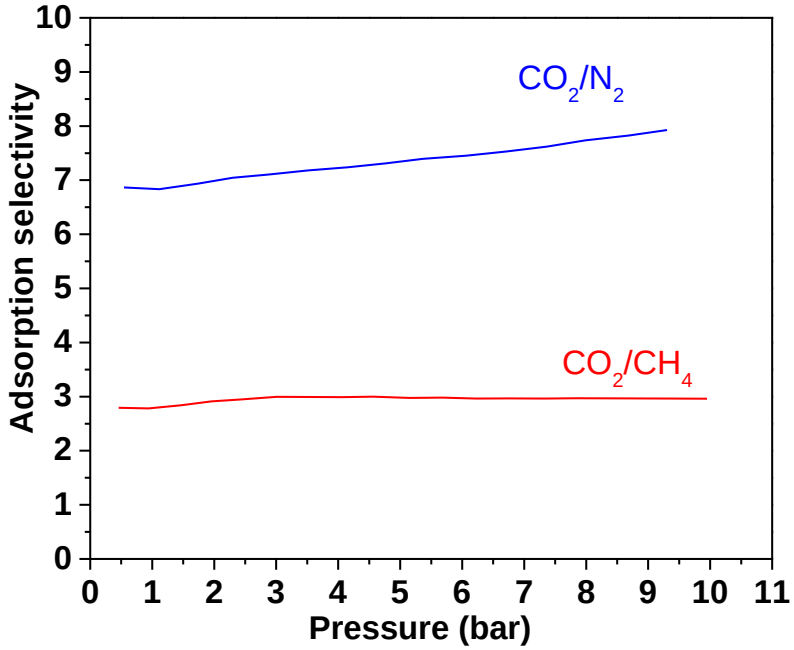

Figure S24. Adsorption selectivity of CO_2 over CH_4 and N_2 on activated **3C** estimated with IAST. The as-made sample (**3C**) was activated before measurements at 70 °C under 10^{-7} mbar

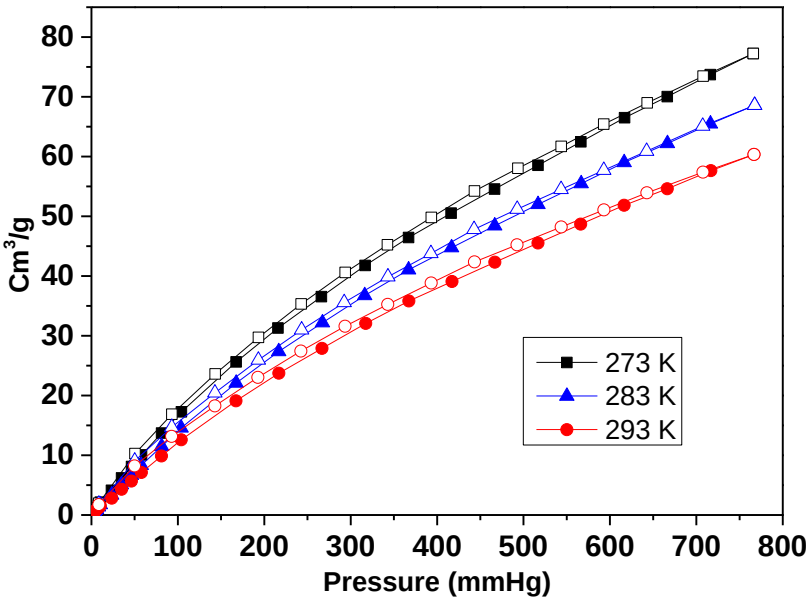

Figure S25. CO_2 adsorption isotherms at 273 K, 283 K and 293 K on activated **3C**. The as-made sample (**3C**) was activated before measurements at 70 °C under 10^{-7} mbar; Filled and empty symbols stand for adsorption and desorption, respectively.

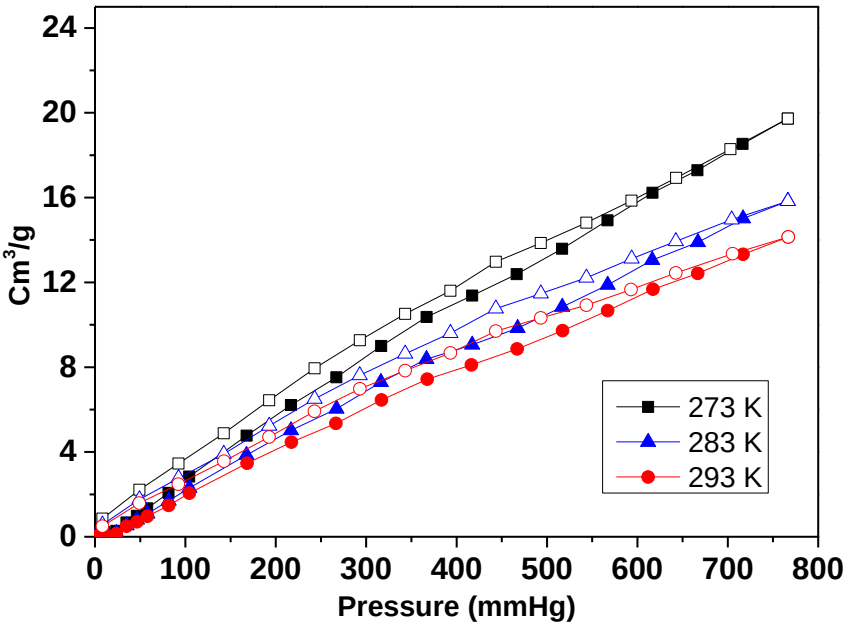

Figure S26. CH_4 adsorption isotherms at 273 K, 283 K and 293 K on activated **3C**. The as-made sample (**3C**) was activated before measurements at 70 °C under 10^{-7} mbar; Filled and empty symbols stand for adsorption and desorption, respectively.

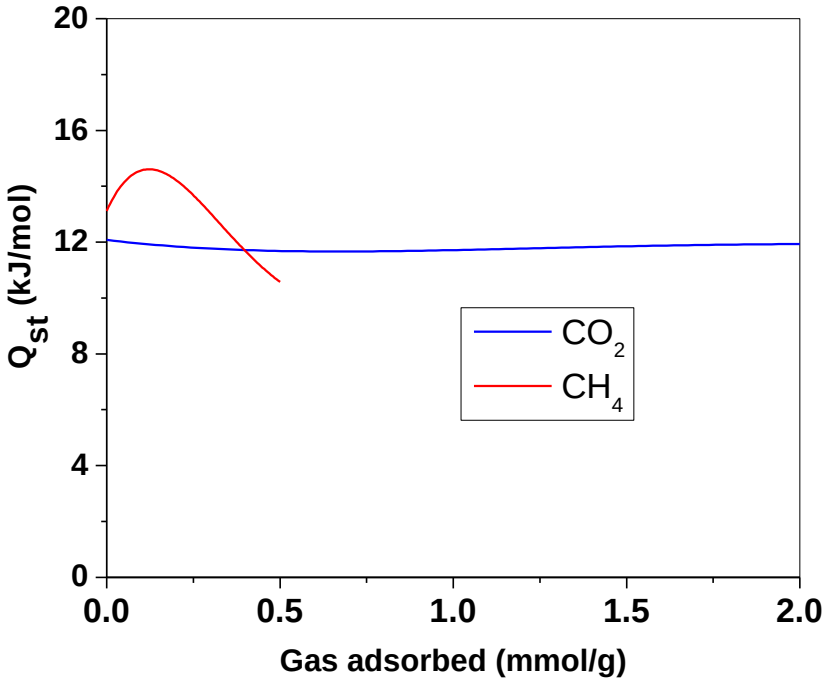

Figure S27. Isosteric heats of CO_2 and CH_4 calculated from the adsorption branches with a virial-type equation for activated **3C**

Heat of Adsorption[2]

CO_2 and CH_4 adsorption isotherms were measured at 273, 283 and 293 K. The collected data for each sample was fitted to virial equation (9)

$$\ln p = \ln v + \frac{1}{T}(a_0 + a_1 v + a_2 v^2 + a_3 v^3 + a_4 v^4) + b_o + b_1 v \qquad (9)$$

where p is the pressure in mmHg, v is the adsorbed amount in $mmolg^{-1}$, T is the temperature in K and a_i and b_i are adjustable parameters.

The isosteric heat of adsorption, Q_{st}, for each gas was calculated according to the equation (10)

$$Q_{st} = -R\,(a_0 + a_1 v + a_2 v^2 + a_3 v^3 + a_4 v^4) \qquad (10)$$

where R is the gas constant in $Jmol^{-1}K^{-1}$.

Ideal Adsorption Selectivity Theory (IAST)[3]

The single component adsorption isotherms of CO_2, and CH_4 collected at 293 K were fitted with the virial type equation (1)

$$P = \frac{n^a}{K} \exp\,(C_1 n^a + C_2 n^{a^2} + C_3 n^{a^3} + C_4 n^{a^4}) \qquad (1)$$

Where P is the pressure in mmHg, n^a is the adsorbed amount in $mmolg^{-1}$, K is the Henry constant and C_i are the constants of the virial equation.

The free energy of desorption at a given value of temperature and pressure of the gas is obtained from the analytical integration of eq. (2)

$$G(T,P) = RT \int_0^P \frac{n^a}{P} dP = RT\left(n^a + \frac{1}{2} C_1 n^{a^2} + \frac{2}{3} C_2 n^{a^3} + \frac{3}{4} C_3 n^{a^4} + \frac{4}{5} C_4 n^{a^5}\right) \qquad (2)$$

The free energy of desorption is a function of temperature and pressure $G(T,P)$ and describes the minimum work (Gibbs free energy) that required to completely degas the adsorbent surface. For a binary mixture of component 1 and 2 the eq. (3) yields the individual pure loadings n_1^a and n_2^a at the same free energy of desorption

$$G_1(n_1^a) = G_2(n_2^a) \qquad (3)$$

The partial pressure of component 1 and 2 in an ideal adsorption mixture given:

$$P_{Tot} x_1^g = P_1(n_1^a) x_1^a \qquad (4)$$

$$P_{Tot} x_2^g = P_2(n_2^a) x_2^a \qquad (5)$$

$$x_1^g + x_2^g = 1 \qquad (6)$$

$$x_1^a + x_2^a = 1 \qquad (7)$$

Where x_1^g and x_1^a is the molar fraction of component 1 in the gas phase and the adsorbed phase respectively and P_1, P_2 is the pure component pressure of 1 and 2, respectively.

Having solved the eq. (3) – (7) for equimolar gas mixture, $x_1^g = x_2^g = 0.5$, the selectivity for the adsorbates 1 and 2 $S_{1,2}$ were obtained from eq. (8) and plotted as function of total pressure P_{Tot}.

$$S_{1,2} = \frac{x_1^a / x_1^g}{x_2^a / x_2^g} = \frac{P_2}{P_1} \qquad (8)$$

SI 9. Scanning electron microscopy (SEM) images of as-made MOFs

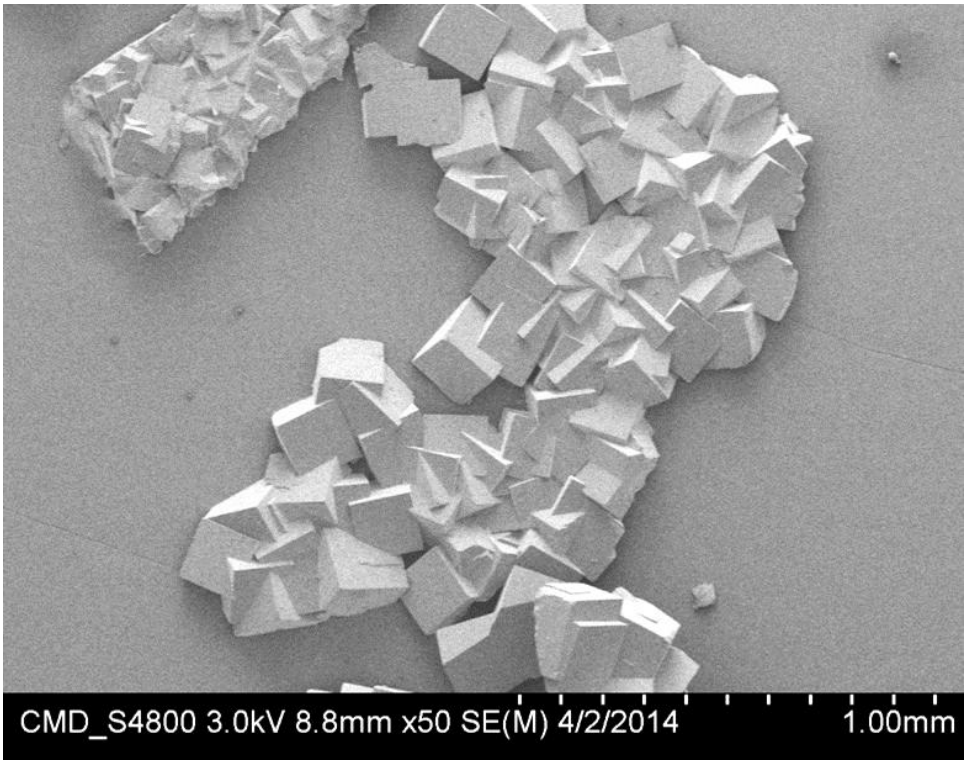

Figure S28. SEM image of as-made **1**

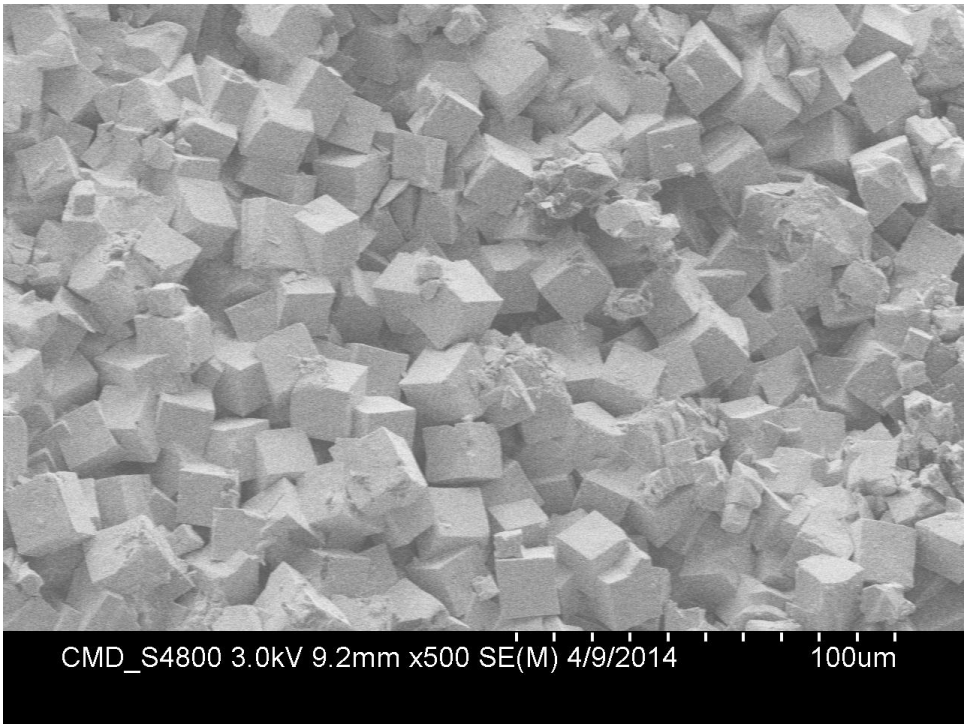

Figure S29. SEM image of as-made **2**

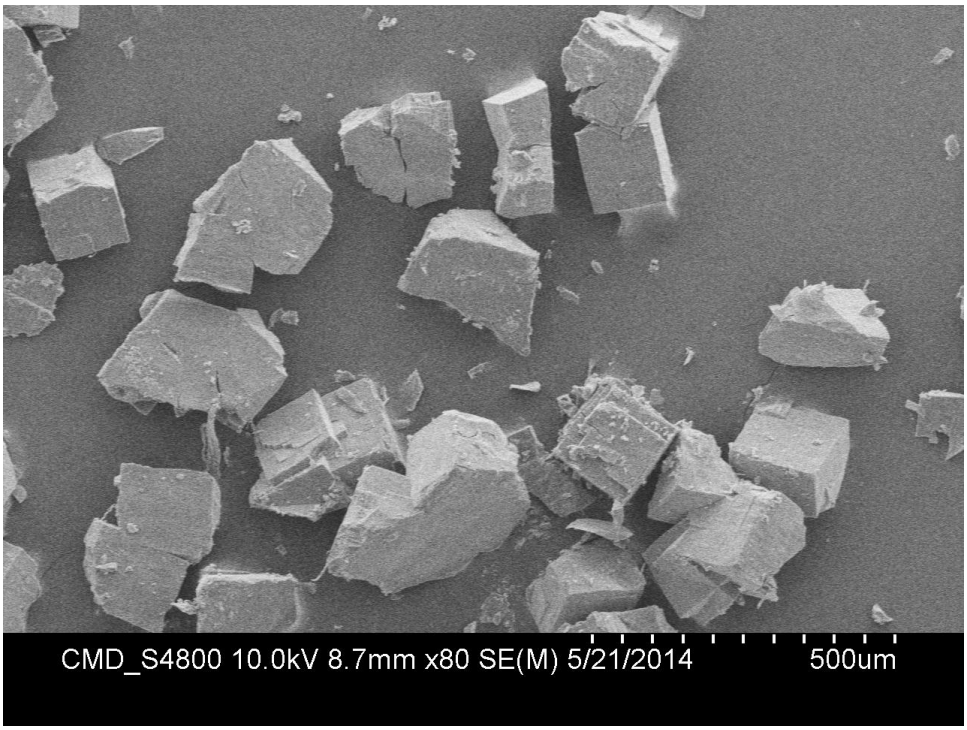

Figure S30. SEM image of as-made **3A**

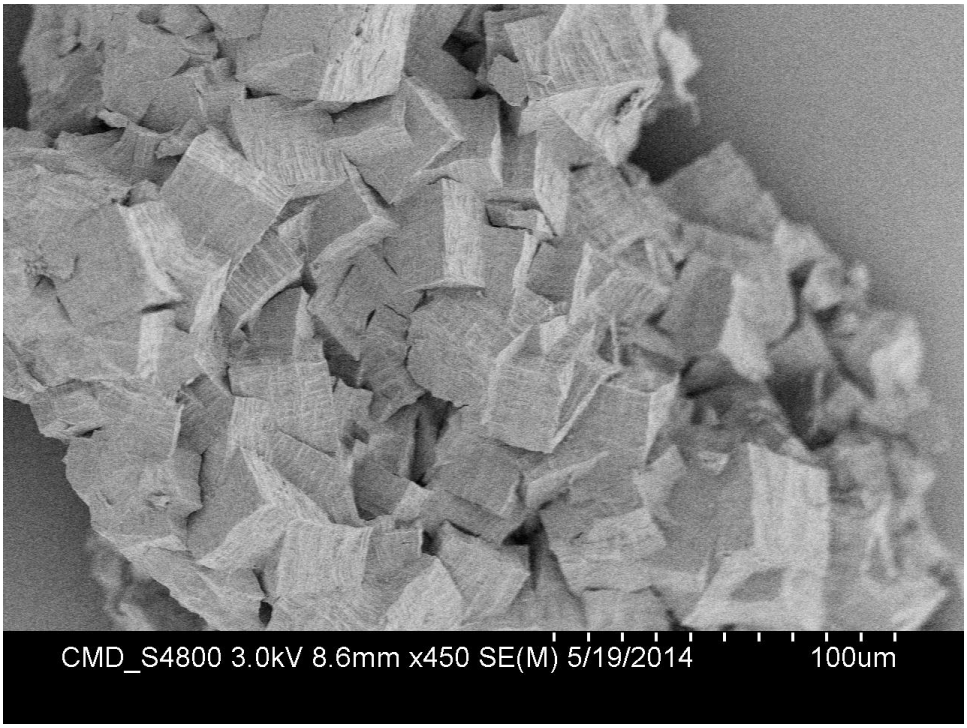

Figure S31. SEM image of as-made **3B**

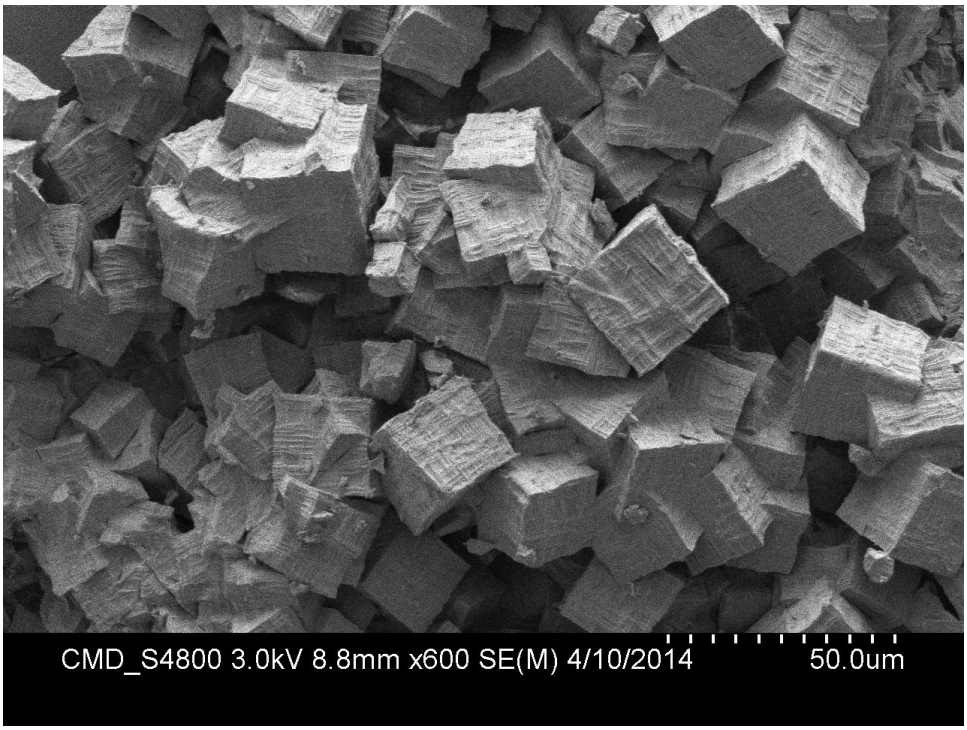

Figure S32. SEM image of as-made **3C**

SI 10. Single Crystal X-Ray Diffraction data collection and analysis

Single-crystal diffraction data were collected using a Rigaku AFC12 diffractometer equipped with a Rigaku Saturn 724+ CCD area detector and 007HF rotating anode Molybdenum source. Samples were mounted under inert oil on Mitegen tips and held under the nitrogen flow from an Oxford Cryosystems cryostream plus. For both **1** and **2** variable-temperature data collections indicated that 250K was the optimum temperature for data collection. A standard data collection comprising of 3x125° ω-scans at 0, 120, 240° settings in φ and common setting of -68° in κ followed by a single 125° scan at κ = -30° and φ = 90° and final low angle 180° ω-scan at κ = φ = 0° was employed for both samples. Data collection on compounds **1** and **2** were undertaken at 1° scan width in ω. For **2** the sample had begun to degrade by the end of the second run, runs 3-5 still had diffraction but at lower resolution but with significantly increased spot size so only runs 1 and 2 were used for structure solution and refinement. The raw frames from the experiments were converted using FMD[8] and processed using APEXII[9]. The converted data was integrated and reduced using SAINT[10] with absorption and scaling correction being undertaken with the program SADABS[11.] Using Olex2[12a], the structure was solved with SHELXS[13] using Direct Methods or Olex2.Solve[11b] and refined with ShelXL[9] using Least Squares minimisation (see CIFs for further details).

a) Compound 1

A slightly green prismatic crystal with dimensions 0.255 x 0.233 x 0.131 mm was selected under inert oil and mounted on a MiTeGen tip and placed under a nitrogen flow on the diffractometer at 250K. Data collection and processing were undertaken as described above. The crystal system is metrically cubic with the space group assigned as $Pm\bar{3}m$ by XPREP [14] and a trial model could be solved for this space group but the degree of disorder of the linker prevented a stable and workable model being obtained. Alternative solutions in $P\bar{1}$, $R\bar{3}$:r, $P\bar{3}$ and $P\bar{3}m$ were explored with the triclinic and $R\bar{3}$:r solutions clearly showing the nature of the linker disorder, solution and refinement of the structure therefore proceeded in $R\bar{3}$:r. Dynamic squeezing was applied to the structure in $R\bar{3}$:r which improved the Rf by 1 % but the HKL file produced had significant completeness issues. Using SQUEEZE in PLATON[15] sees an improvement of 0.4 % but without compromising data completeness. It was necessary to apply SIMU, DELU and ISOR restraints to the ADPs for all carbon atoms as there is a pronounced elongation of the ADPs in the X component becoming larger with distance from the Zr-O bond, the restraints constitute an approximate 0.2 % Rf penalty for doing so. Attempts to split the model in this plane were unsuccessful in $R\bar{3}m$:r and $R\bar{3}$:r and are suggestive of a relatively high degree of displacement in the ligand plane. Attempts to split the disorder in $P\bar{3}m$ also proved to be unstable while normal use of the PART -1 command destroyed the model on refinement in $R\bar{3}m$. $Pm\bar{3}m$ is a minimal non-isomorphic supergroup of $R\bar{3}m$ and $R\bar{3}m$ is a minimal non-isomorphic supergroup of $R\bar{3}$:r. Hydrogens were fixed using AFIX 43 and the occupancies based on the thermal parameter of the parent atom, from chemical analysis the formula of the SBU is $Zr_6O_4(OH)_4$, in the crystal structure the Zr1-O2 and Zr1-O3 bond lengths are equal suggesting that both oxygen positions correspond to partial occupancy by O and OH, the hydrogen atoms have not been modelled at these positions but have been included in the unit cell contents Pictures for the

manuscript were created using the structure in R$\bar{3}$:r with a single component of the disorder shown.

b) Compound 2

An orange prismatic crystal with dimensions 0.068 x 0.058 x 0.052 mm was selected under inert oil and mounted on a MiTeGen tip and placed under a nitrogen flow on the diffractometer at 250K. Data collection and processing were undertaken as described above. The crystal system is metrically cubic with the space group assigned as Pm$\bar{3}$m by XPREP and a trial model can be solved for this space group. However the degree of disorder of the linker makes a stable and workable model very difficult. Alternative solutions in P$\bar{1}$, R$\bar{3}$:r, P$\bar{3}$ and P$\bar{3}$m were explored with the triclinic and R$\bar{3}$:r solutions clearly showing the nature of the linker disorder, solution and refinement of the structure therefore proceeded in R$\bar{3}$:r.. It has also been necessary to apply SIMU, DELU and ISOR restraints to the ADPs for all carbon atoms as there is a pronounced elongation of the ADPs in the X component becoming larger with distance from the Zr-O bond, attempts to split the model to model the disorder in this component were unsuccessful in R$\bar{3}$:r and are suggestive of a relatively high degree of displacement in the ligand plane. The restraints constitute an approximate 0.5 % Rf penalty for doing so. From data collections undertaken at temperatures of 100K to 200K in 50K increments we were unable to resolve the two-fold rotational disorder in the ligand as clearly as in the 250 K data set. Attempts to split and model the disorder in P$\bar{3}$m also proved unstable. It was found that the normal use of PART -1 destroyed the model on refinement in SHELXL. The final refinement was completed in R$\bar{3}$:r as this allows for the two PARTs of the disorder to be readily isolatable and produced a stable model with low Rf and relatively few (52) inconsistent reflections. Pm$\bar{3}$m is a minimal non-isomorphic supergroup of R$\bar{3}$m and R$\bar{3}$m is a minimal non-isomorphic supergroup of R$\bar{3}$:r. It is possible to solve and refine this structure in R$\bar{3}$m:r however the final model is difficult to deconvolute. Pictures for the manuscript were created using the structure in R$\bar{3}$:r which allows for the use of PART 1 and PART 2 to separate out the disorder into two components although it is logical to conclude this is an oversimplification of the actual situation.

In addition to the twofold rotational disorder there is disorder evident from the difference map that is suggestive of rotation of the pyrene core about its longest axis, resulting in one conformation where it lies out of plane with respect to the benzoate groups. This is observed as “buckling” of one of the pyrene cores relative to the plane of the benzoate groups as shown in **Figure S34(iv)**. The model was expanded, the symmetry generated atoms converted and the ring held in place using a riding model based on Ilia A. Guzei’s fragment database[16]. This was repeated for all ring components expect atom C4, C5, C4' and C5'. The positions of these atoms were fixed by DFIX and DANG restraints. A FLAT restraint was applied to both of the grown disordered pyrene fragments and the first pendant carbons followed by a separate FLAT applied to the benzoates and first pendant carbons. Hydrogens were fixed using AFIX 43 and the occupancies based on the thermal parameter of the parent atom. From chemical analysis the formula of the SBU is $Zr_6O_4(OH)_4$, in the crystal structure the Zr1-O3 and Zr1-O4 bond lengths are equal suggesting that both oxygen positions correspond to partial occupancy by O and OH, the hydrogen atoms have not been modelled at these positions but have been included in the unit cell contents once the model had converged and was stable the

AFIX 3 flags were removed and the refinement repeated. This reduced the Rf and the model proved to be stable. Finally dynamic squeezing was applied to the data as part of the Olex2 refinement package for the model in R$\bar{3}$:r, which improved the Rf by 2%.

Table S4: Crystal data and refinement parameters for structures **1** and **2**.

Identification code	sntD0072c2	sntD0073c3
Sample Code	1	2
CCDC	1006810	1006811
Empirical formula	$C_{144}H_{70}O_{36}Zr_6$	$C_{156}H_{70}O_{36}Zr_6$
Formula weight	2923.32	3067.44
Temperature/K	250(2)	250(2)
Crystal system	Cubic*	Cubic*
Space group	R$\bar{3}$:r *	R$\bar{3}$:r *
a/Å	22.071(10)	21.983(4)
b/Å	22.071(10)	21.983(4)
c/Å	22.071(10)	21.983(4)
α/°	90.00	90.00
β/°	90.00	90.00
γ/°	90.00	90.00
Volume/ $Å^3$	10752(8)	10624(4)
Z	1	1
Pcalc mg/mm^3	0.451	0.479
μ/mm^{-1}	0.165	0.168
F(000)	1462.0	1534.0
Crystal size/mm	0.255 x 0.233 x 0.131	0.068 x 0.058 x 0.052
2θ range for data collection	1.84 to 53.44°	1.86° to 51.02°
Index ranges	$-23 \leq h \leq 27$, $-24 \leq k \leq 27$, $-27 \leq l \leq 23$	$-26 \leq h \leq 15$, $-26 \leq k \leq 25$, $-26 \leq l \leq 22$
Reflections collected	93215	49464
Independent reflections	15145[R(int) = 0.1249]	12889 [R(int) = 0.1550]
Data/restraints/parameters	15145/831/414	12889/968/520
Goodness-of-fit on F^2	1.063	0.872
Final R indices [I>=2σ(I)]	R_1= 0.0552, wR_2= 0.1612	R_1= 0.0509, wR_2= 0.1327
Final R indices [all data]	R_1= 0.0857, wR_2= 0.1822	R_1= 0.0756, wR_2= 0.1383
Largest diff. peak/hole /$eÅ^{-3}$	1.32/-0.64	0.42/-0.78

* XPREP assigned both structures as Pm$\bar{3}$m, however in order to enable a stable refinement of the ligand disorder both were solved and refined in R$\bar{3}$:r. Full details are given in SI 10

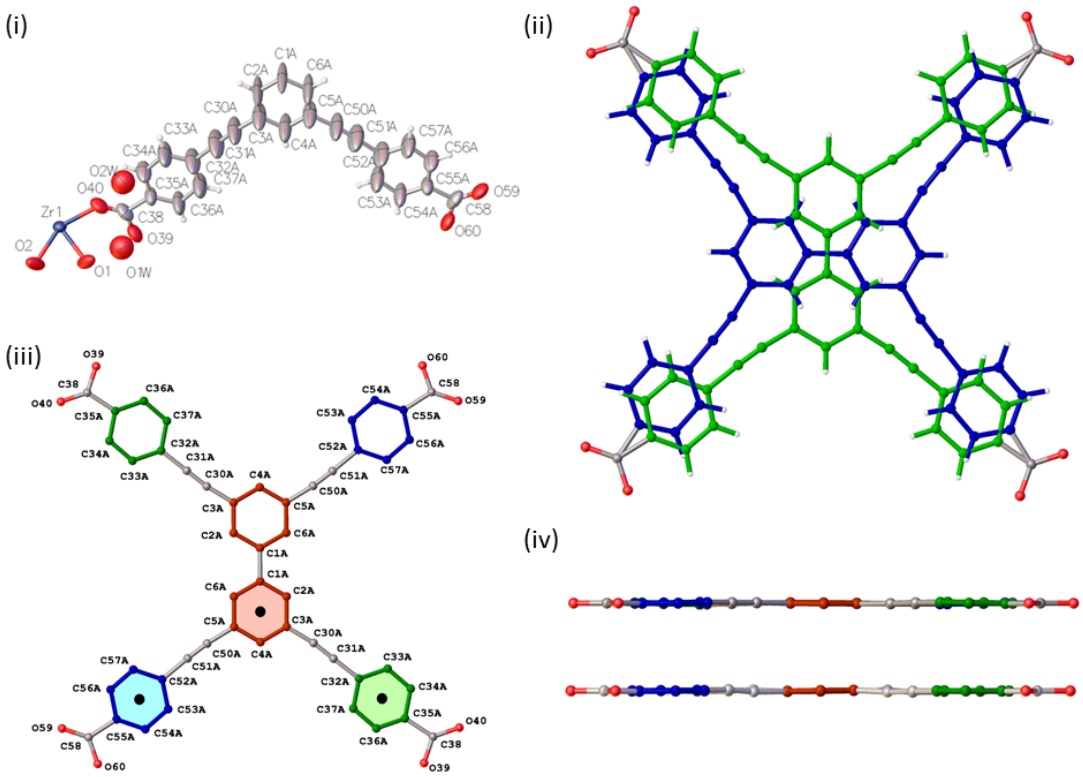

Figure S33: (i) Asymmetric unit of **1** with thermal ellipsoids shown at the 50% probability level, for clarity only one position for the disordered BTPBA ligand is shown, (ii) overlay of the two crystallographically-distinct linker conformations showing the two-fold rotational disorder, (iii) atom numbering scheme for one linker conformation, (iv) both linkers viewed along their planes.

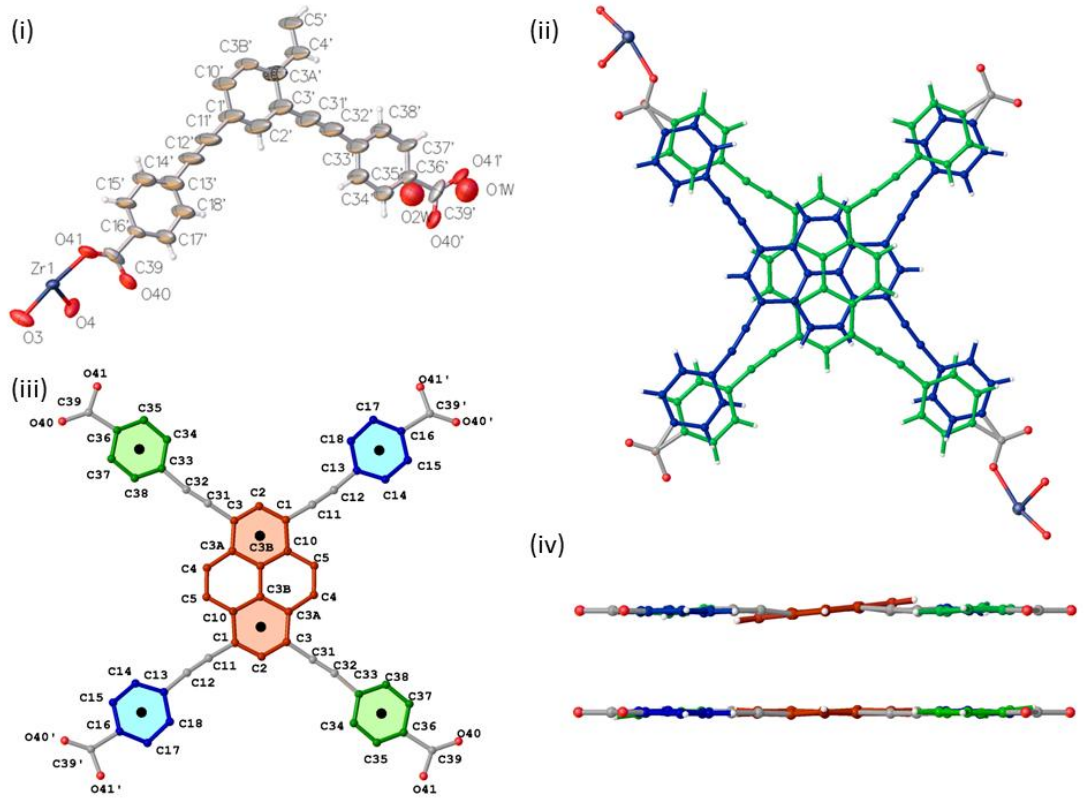

Figure S34: (i) Asymmetric unit of **2** with thermal ellipsoids shown at the 50% probability level, for clarity only one position for the disordered BTPBA ligand is shown, (ii) overlay of the two crystallographically-distinct linker conformations showing the two-fold rotational disorder, (iii) atom numbering scheme for one linker conformation, (iv) both linkers viewed along their planes.

C) Effect of linker disorder on window size and porosity of 1 and 2

The two-fold rotational disorder of the linker molecules in **1** and **2** results in the possibility of formation of two distinct microporous cage structures consisting of a single linker component where all the linkers on the faces of the cube are symmetry equivalent or alternating linkers from both disorder components on neighboring faces. These two cases correspond to the "symmetric" and "asymmetric" linker combinations respectively that are used as the basis of the DFT calculations and these are shown schematically in **Figure S36** (*vide infra*). In the symmetric case a single window type is present in each cage corresponding to the neighboring linkers lying orthogonal to each other while in the asymmetric case two additional window types are present, one where the linkers lie parallel with the longest axis of the biphenyl or pyrene cores along the SBU-SBU axis and a second with the longest axes of the linker cores lying along a common axis pointing towards the centre of the window (Figure 1d, main text). The differences in linker orientation have the effect of reducing the maximal width of the window along the linker-linker axis, when these are measured from the closest interatom contact distances between the biphenyl or pyrene cores this results in a reduction from 12.783(4) Å for the parallel window to 11.815(4) Å for the orthogonal window to 9.272(3) Å for the common axis widow in 1 with corresponding values of 11.2662 (13) Å, 10.4134 (13) Å and 9.334(12) Å in **2**. However, it should be noted in all these cases that the minimal window dimension corresponds to the distance across the diagonal between the

benzoate groups of two linkers, which is approximately 2 Å shorter than the maximal distance along the central linker-linker axis. The maximum radius of a spherical probe that could penetrate each window type was calculated using the CALCVOID function implemented in Olex2 with a resolution of 0.05 Å. In the symmetric **1** the probe radius was 3.75 Å for the orthogonal windows whereas in the asymmetric unit the parallel and common axis windows probe radii were reduced to between 3.25Å and 3.35 Å, with no correlation between these values and the parallel or common axis windows. The total solvent accessible void volume was 8664.3 $Å^3$ (80.6 % of the unit cell) for the symmetric **1** cage and 8193.0 $Å^3$ (76.2% of the unit cell volume) for the asymmetric **1**, with no reduction in the effective pore diameters of the two cages. In **2** the window sizes were 3.75 Å for the orthogonal window and 3.30 Å for the parallel and common axis windows. The total solvent accessible void volumes of are 8386.0 $Å^3$ (78.9 % of the unit cell volume) for the symmetric cage and 8049.0 $Å^3$ (75.8% of the unit cell volume) for the asymmetric cage with maximum effective pore diameters for the microporous cages in **2** of 18.5 Å.

SI 11. Molecular Dynamics (MD) simulations of linker flexibility

To compare the flexibility of the $btbaH_4$ and $ptbaH_4$ linkers we conducted a series of constrained molecular dynamics (MD) simulations using the MMFF96 force field as implemented in the molecular modelling package Avogadro.[17] In each simulation the angle between the upper and the lower part of the linker shown in **Figure S35a** was constrained and the molecule was allowed to relax. The corresponding energy profile is shown in Figure S1b for both $btbaH_4$ and $ptbaH_4$ linkers. There is only one minimum energy configuration for the $ptbaH_4$ linker at zero degrees, corresponding to the planar linker. In contrast, the planar conformation is not energetically favourable for the $btbaH_4$ linker: the free linker adopts a twisted conformation with a torsion angle of 53°. While DFT calculations predict a torsion angle of 38.5 °and energy barriers of 8.0 kJ/mol at zero degrees and 8.3 kJ/mol at 90 ° for a free biphenyl molecule,[18] the qualitative behaviour is the same as seen in our MD simulation for the $btbaH_4$ linker: the biphenyl core allows the upper and the lower parts of the linker to rotate with respect to each other, whereas rotation is much more restricted in the case of the pyrene core.

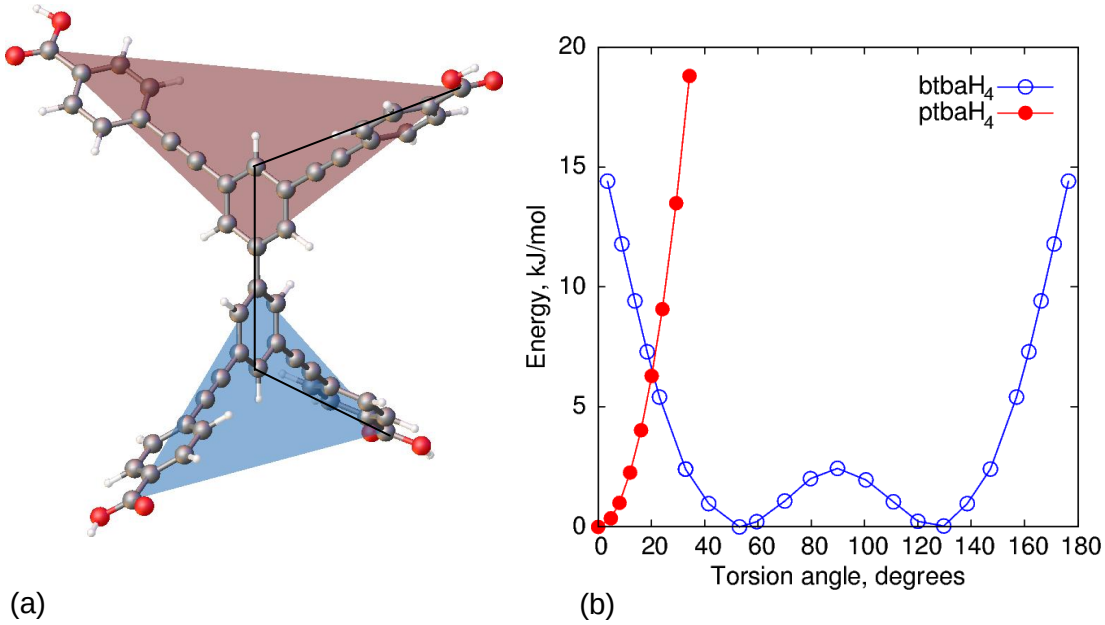

Figure S35: a) the conformation of the $btbaH_4$ linker with a 90° torsion angle between the upper and the lower part of the molecule as defined by the dihedral angle shown. (b) Energy profile with respect to the torsion angle defined above for both $btbaH_4$ and $ptbaH_4$ linkers.

SI 12. Density Functional Theory (DFT) calculations

3D-periodic DFT calculations of a single unit cell containing 3 linkers and 1 zirconium SBU were performed with the Vienna ab initio Simulation Package (VASP)[19] version 5.3.3. The PBE functionals were used in the framework of Projector Augmented Wave method[20] and the Generalised Gradient Approximation.[21] The specific settings used for the VASP calculations were:

- Gaussian smearing was used with smearing width of 0.1 eV.
- The "accurate" precision setting was used with convergence criteria of $1x10^{-5}$ eV for the electronic energy convergence and 10^{-3} eV/Å for the residual force for the ionic convergence.
- The cut-off energy of 600eV was used throughout
- The method of conjugate gradients was used to optimise the ion positions, cell volume and cell shape, with force scaling factor of 0.1. The simulations were typically run for the total of 1000 ionic relaxation steps and periodically restarted to remove the accumulative error in energy arising from varying the cell dimensions.
- All calculations were performed using the first First Brillouin Zone, e.g. under Gamma point approximation.
- The van der Waals interactions were taken into account by the vdW-DF method developed by Dion *et. al*[22].

The geometry optimisation calculations for 3d periodic structures were started from experimental coordinates altered randomly by 0.05 Å to allow the relaxation under C1 point symmetry. Thus all cell parameters and ionic positions were optimised independently under no symmetry constraints. The four hydrogens were manually added to the zirconium SBU to

provide correct charge balance and stoichiometry of $Zr_6O_4(OH)_4$. The arrangement of the hydrogen atoms on each SBU is controlled by electrostatic forces. The μ_3-O position is preferred by hydrogen monoatoms over the μ_2-O due to the larger negative charge on the 3-fold site, ~0.12e greater on the μ_3-O than the μ_2-O according to Mulliken charge analysis. Positioning the hydrogen atoms at maximal separation from one another, capping opposing vertices of the tetradecagonal SBU, minimises OH….OH dipole interactions and gives rise to an apolar SBU. There are two isoenergetic configurations for each SBU hence the average occupancy for a hydrogen site bonded to each μ_3-O is 0.5. Positioning the four hydrogen atoms at minimum separation from one another on the SBU incurs an energetic penalty of +41 kJ/mol per hydrogen and results in a polar SBU and is therefore strongly disfavoured.

There are two distinct possible ways of arranging three linkers with axial symmetry within a 3D periodic unit cell as schematically shown in **Figure S36**. Both cases were considered for each linker.

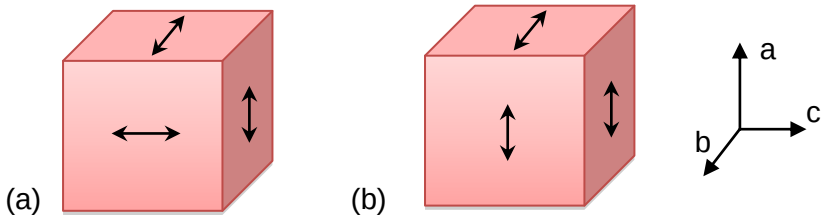

Figure S36. The schematic representation of a symmetric (a) and asymmetric (b) 3D periodic unit cell for either the btba or ptba linker. Here the arrows show the orientation of either biphenyl or pyrene core for each linker.

Table S5. Unit cell parameters of symmetric and asymmetric structures

Unit cell	**a, Å**	**b, Å**	**c, Å**	**A, °**	**B, °**	**C, °**	**V, Å^3**
biphenyl core symmetric cell	22.178	22.178	22.178	90.00	90.00	90.00	10908.79
biphenyl core asymmetric cell	22.314	22.165	22.085	90.00	90.00	90.01	10923.32
pyrene core symmetric cell	22.253	22.253	22.253	89.99	89.99	89.99	11019.73
pyrene core asymmetric cell	22.340	22.237	22.167	89.99	89.99	90.01	11011.71

The four structures were optimised using the vdw-DF method with parameters given above. For the symmetric structures, both biphenyl- and pyrene-containing unit cells adopted cubic geometry, i.e. a=b=c and A=B=C=90° as can be seen in the **table S5**. The lowest space group symmetry present in these symmetric cells was identified as R3 by using FindSym.[23] Similarly both asymmetric cells were found to adopt orthorhombic geometry with underlying P222 space group symmetry. The latter simply indicates that while all three linker

conformations are slightly different from each other (as can be seen by the fact that a≠b≠c in the asymmetric cells), each of the four linker arms have the same conformation for a given linker.

Table S6. The energies and the linker core geometry in the DFT calculated structures

Unit cell	Energy, eV	ΔE, kJ/mol	core twist, °
biphenyl core symmetric cell	-1861.731		24.56
biphenyl core asymmetric cell	-1861.721	+1.05	26.48, 22.29, 20.70
pyrene core symmetric cell	-1974.087		1.66
pyrene core asymmetric cell	-1974.059	+2.78	1.85, 1.58, 1.43

The absolute energies calculated using the vdW-DF method are shown (**Table S6**) for the whole unit cell containing one zirconium SBU and three linkers. The energy difference between the symmetric and the asymmetric cells, e.g. the energy penalty for the rotation of an individual linker by 90°, was found to be of only a few kJ/mol for both byphenyl and pyrene structures. This suggests that there is negligible correlation between the orientation of neighbouring linkers and their orientation can be considered to be random throughout the experimental MOF structures. The angle between the planes of the phenyl rings in the byphenyl core is shown together with the analogous angle measured in the pyrene core. For the asymmetric cells the angles are given for each of the three distinct linker conformations in order (a, b, c) consistent with **Figure S36b**. The calculated linker conformations are consistent with the experimental data with the conformational flexibility accounted for by the elongation thermal ellipsoids along the normal of the ligand plane. The thermal ellipsoids at the 50% probability level in both structures account for the DFT calculated atom positions for the symmetric cells as shown in **Figure S37 and S38**.

Table S7. The Zr-O distances in the SBU as observed in DFT calculated structures. Note that in both btba and the ptba structures, there are two distinct Zr-O distances depending on whether the oxygen belong to an oxo or hydroxo group. There are also two Zr-O (carboxylate) bond lengths. This difference in bond length arises because of the struts connecting the SBUs and the linker core in both biphenyl and pyrene case do not form a 45° angle with the axis of the unit cell, whereas the symmetry of the SBU demands the 45° orientation. To alleviate this geometric frustration, the strut bends as shown in **Figure S37** and **Figure S38**. Therefore, in both structures two distinct Zr-O (carboxylate) bond lengths are observed.

Unit cell	Zr-O (oxo) (Å)	Zr-O (hydroxo) (Å)	Zr-O (carboxylate) (Å)
biphenyl core symmetric cell	2.099	2.295	2.212 and 2.315
pyrene core symmetric cell	2.098	2.296	2.210 and 2.319

We also performed vdW-DF calculations for a single $btbaH_4$ and $ptbaH_4$ linkers in the gas phase to compare their longitudinal and lateral dimensions to those calculated for the MOF structure and observed experimentally in **1** and **2**. The axis parallel to the C-C bond connecting the phenyl rings in the biphenyl core of the $btbaH_4$ linker, i.e. the vertical axis in Scheme 1 of the main text, corresponds to the longitudinal axis. The distances between carbons from the carboxylate groups are reported in angstrom in the table below:

Table S8. The calculated distances between carbons from carboxylate groups along the longitudinal and lateral axes for free $btbaH_4$ and $ptbaH_4$ linkers in a gas phase and those in the symmetric and asymmetric cells as described above. The lateral dimension of the free $btbaH_4$ linker, 16.023 Å, is slightly larger than other values reported in the table due to the 18.6° twist of the biphenyl core. The experimental values reflect the two-fold rotational linker disorder present in the structure where the longitudinal and lateral linkers were modelled with common carboxylate positions that could not be resolved into the individual components.

	biphenyl linker		**pyrene linker**	
	longitudinal**(Å)**	lateral**(Å)**	longitudinal**(Å)**	lateral**(Å)**
free linker	15.598	16.023	15.846	15.814
symmetric cell	15.846	15.673	15.913	15.733
asymmetric cell	15.803 15.897 15.929	15.638 15.664 15.684	15.869 15.921 15.948	15.715 15.735 15.745
experiment	15.759(9), 15.760(9)		15.689(7), 15.707(7)	

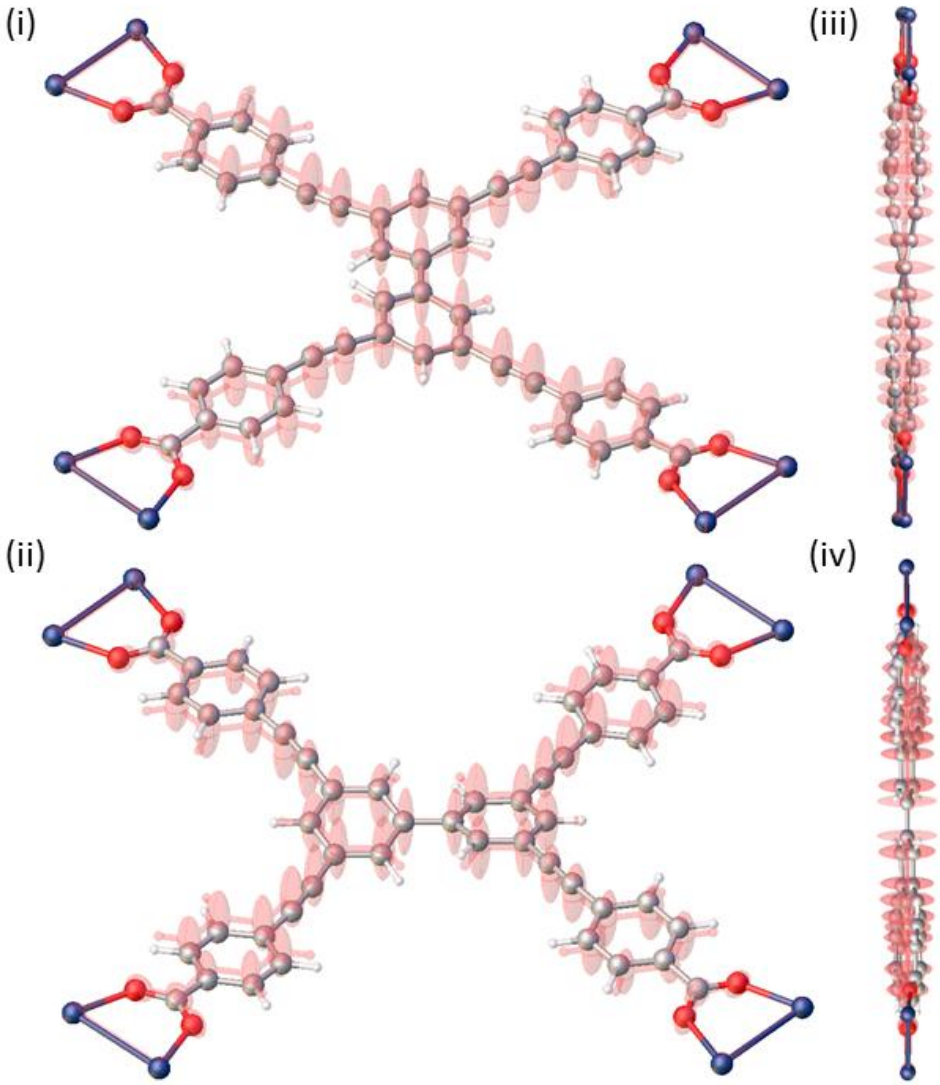

Figure S37: Overlay of the calculated symmetric cell linker conformation for the btba-linker with the experimental crystal structure. The overlay was calculated from the Zr atom positions. The displacement ellipsoids for the carbon atoms are shown at the 50 % probability level. Figure (iii) shows the view along the common plane of (i) rotated 90° around the vertical plane of the page while (iv) shows the view along the common plane of (ii) rotated 90° around the vertical plane of the page.

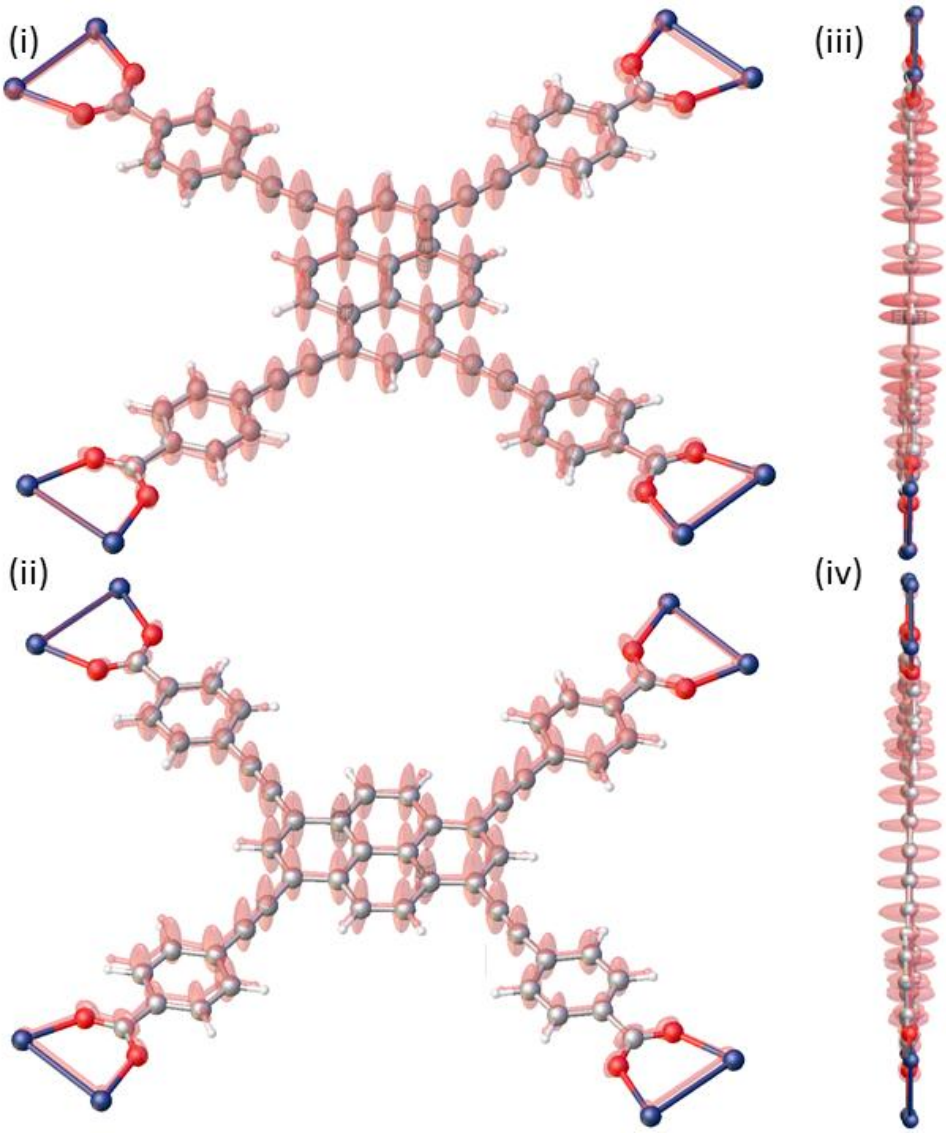
(i)
(iii)
(ii)
(iv)

(v)

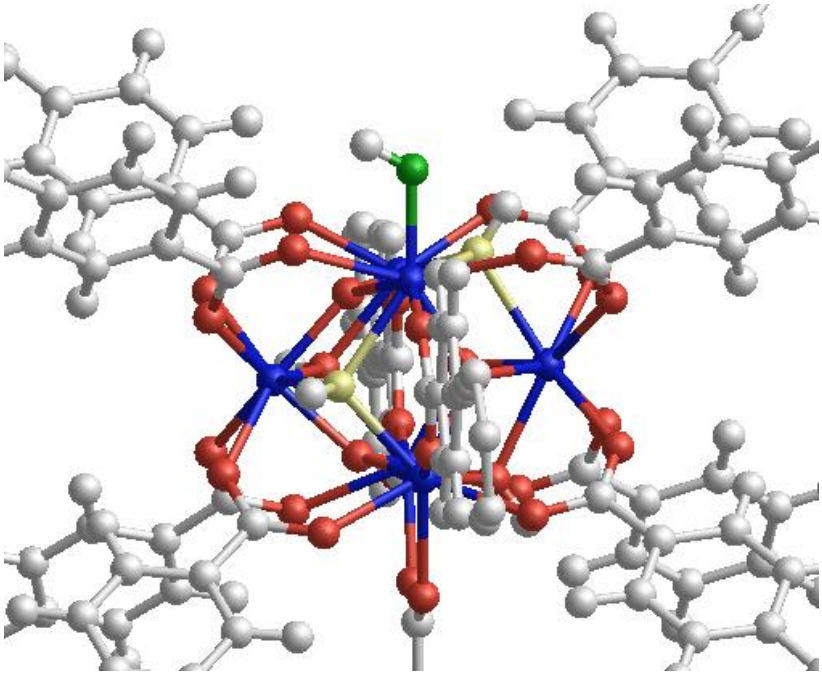

Figure S38: Overlay of the calculated symmetric cell linker conformation for the ptba-linker with the experimental crystal structure. The overlay was calculated from the Zr atom positions. The displacement ellipsoids for the carbon atoms are shown at the 50% probability level. Figure (iii) shows the view along the common plane of (i) rotated 90° around the vertical plane of the page while (iv) shows the view along the common plane of (ii) rotated 90° around the vertical plane of the page. (v) highlights the geometry around the defective ptba material, where a missing linker is compensated by an OH^- (emphasised in green) and two neighbouring μ_3-O species, displayed in yellow.

To examine the effect of missing linkers on the water stability of **2** a separate DFT study was performed using the Quickstep module of the CP2K software (www.cp2k.org). The PBE functional was used with Grimme's D3 correction (http://www.thch.uni-bonn.de/tc/index.php?section=downloads&subsection=DFT-D3&lang=english) to account for non-local dispersive interactions. A cutoff of 550 Ry and a cubic reference cell of length 23.5Å was used. As already noted, the Zr-O(carboxylate) distances are unequal in length and it is presumed the longer of the two bonds binding the linker to the Zr is more vulnerable to attack from water. In defective **2**, a missing linker is compensated by an OH^- group, which is attracted to the electropositive undercoordinated Zr site, as shown in **Figure S38**. Since this Zr site is additionally attached to 2 μ_3-OH groups, it was speculated that the presence of the compensating OH^- may activate the structure to water attack.

A 2x2x2 supercell was constructed where a single pbta ligand was replaced by 4 OH^- groups and the structure relaxed at fixed cell parameters. Upon relaxation, it was found that the three Zr-O(carboxylate) bonds at the Zr site as depicted in **Figure S38** change from 2.27, 2.24 and 2.28 Å to 2.19, 2.31 and 2.34 Å respectively; one bond strengthens and two bonds weaken. To assess the impact of this defect on water stability, first, anhydrous forms of structures **1** and **2** were optimized to equilibrium density without constraints on cell symmetry. Next, the longer of the two Zr-O(carboxylate) bonds bound to a Zr was manually broken and the phenyl moiety rotated to allow one of the O(carboxylate) atoms to coordinate to a μ_3-OH, whilst retaining a single connecting Zr-O(carboxylate) bond. For structures **1** and **2** this defect,

which is presumed to be a step in the leaching of Zr, incurs a penalty of +46 kJ/mol and +48 kJ/mol respectively. The same process was repeated in the OH^- compensated structure and the defect formation energy was found to be lowered to +7 kJ/mol. The same process was repeated but in the presence of 2 water molecules coordinated to the Zr sites of interest. The defect formation energies become +1 and -2 kJ/mol for structures **1** and **2**. For the OH^- compensated structure, breaking the longest Zr-O(carboxylate) bond is more strongly exothermic, yielding -39 kJ/mol. These data suggest that the intrinsic water stability of pristine, stoichiometric **1** and **2** is similar and that it is the presence of defects in the ptba structure which activates the as-synthesized pbta material to water attack.

To further investigate why the **3A** material shows the strongest resilience to attack from water, we constructed 1x1x2 supercell from **1** and exchanged one of the flexible btba ligands for a rigid ptba ligand, which gives a ptba:btba ratio of 16.7%, close to the **3A** ratio of 13.3%. For comparison, we also created a 1x1x2 supercell where half of the flexible btba ligands are exchanged for rigid ptba ligands precisely reproducing the ligand ratio found in **3B**. The **3A**, **3B** and 1x1x2 supercells of **1** and **2** were all optimized to mechanical equilibrium. **Figure S39** shows the Zr-O bond lengths as found in **1**, **2**, **3A** and **3B** which shows three distinct bond length distributions. Around 2.07Å, all materials have very similar Zr-O bond lengths and these correspond to the Zr….μ_3-O distances. **1**, **2**, and **3A** have two very similar distributions of bond length at 2.17-2.19 Å and 2.26-2.3 Å; these correspond to the Zr-O distances between the Zr cluster and the carboxylate oxygen of the ptba or btba linkers. As already discussed (**Table S8**), the inequivalent bond lengths arise because of geometric frustration. **Figure S39** clearly shows that although 1 in 6 of the ligands has been exchanged for rigid ptba, **3A** accommodates the relatively inflexible ligand without deviating significantly from the ideal bond lengths, as found in the end member **1** and **2** materials. The density of **3A** is also slightly higher than **1** suggesting that **3A** should display higher mechanical resilience as is seen experimentally. By contrast, **3B** has a lower density than **3A** but more significantly, the Zr-O bond length distribution of **3B** is qualitatively distinct from the other materials. The shorter Zr-O bond lengths deviate from their ideal lengths of 2.17-2.19 Å to 2.18-2.23 Å whilst the longer bonds decrease from 2.26-2.3 Å to 2.25-2.29 Å. It appears that the increased proportion of ptba in **3B** induces strain that is alleviated by significant distortion of the Zr-O ligand bond lengths away from their ideal values. It is reasonable to suppose that the distorted Zr-O ligand bond lengths render **3B** more susceptible to water attack, explaining why **3A** is water stable whilst **3B** is not.

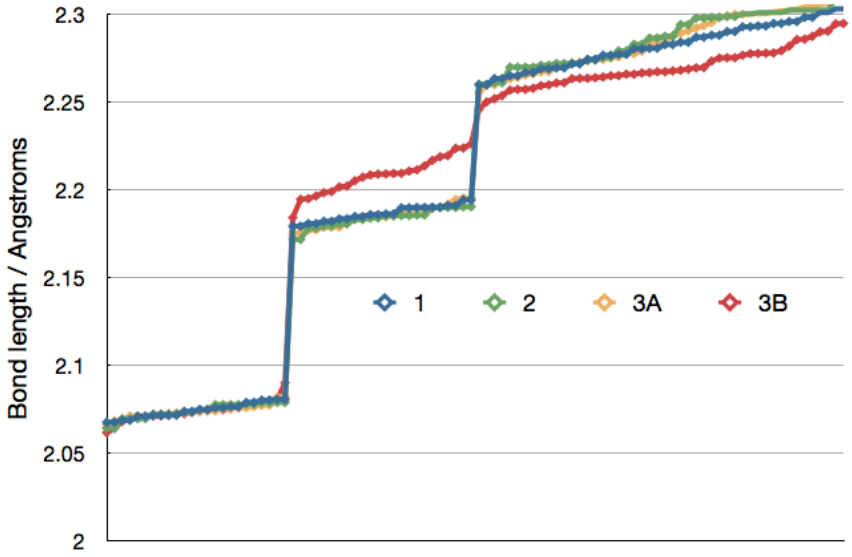

Figure S39. Zr-O bond lengths obtained from the optimized structures of **1**, **2**, **3A** and **3B**. The bond length data has been sorted by magnitude and the lines are guides to the eye.

SI 13 X-Ray Powder Diffraction Data

X-ray powder diffraction data were collected at room temperature for as-made and activated samples of **1**, **2**, **3A, 3B,** and **3C** on a Bruker D8 diffractometer operating in transmission mode using Ge (111) monochromated Cu $K\alpha_1$ radiation. Samples were loaded into 0.7mm borosilicate glass capillaries. Data were collected in the range 3 to 40 degrees 2θ. Lattice parameters for the phases were obtained by Pawley fitting of the data using Topas Academic with starting unit cell parameters taken from the single-crystal diffraction data.

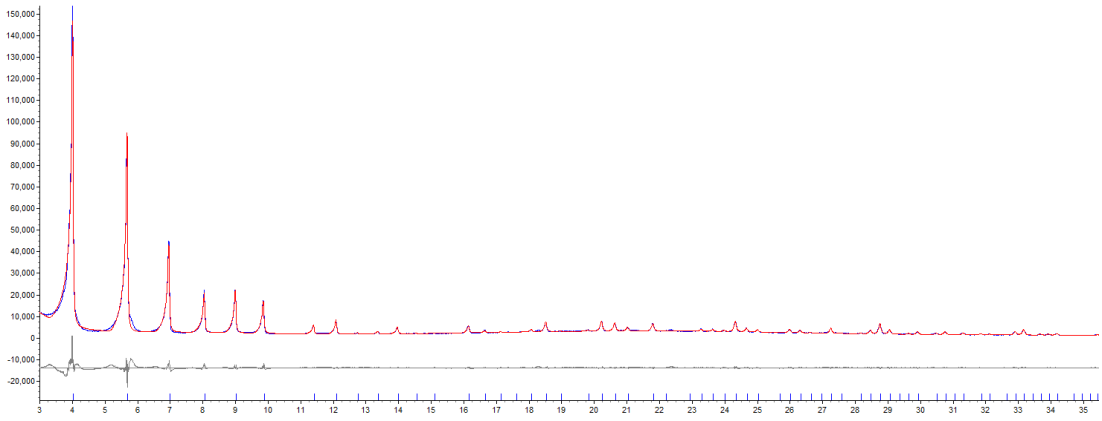

Figure S40. Experimental (blue line), calculated (red line) and difference plot (grey line) for Pawley fitting of the diffraction data obtained for as-made **1** in cubic space group $Pm\bar{3}m$ with refined values of a/b/c= 21.916(1) Å. The indexed peak positions are shown by the blue tick marks. R_{wp}= 7.68%, R_{exp}= 1.57%, R_p= 5.25%, χ^2= 4.88.

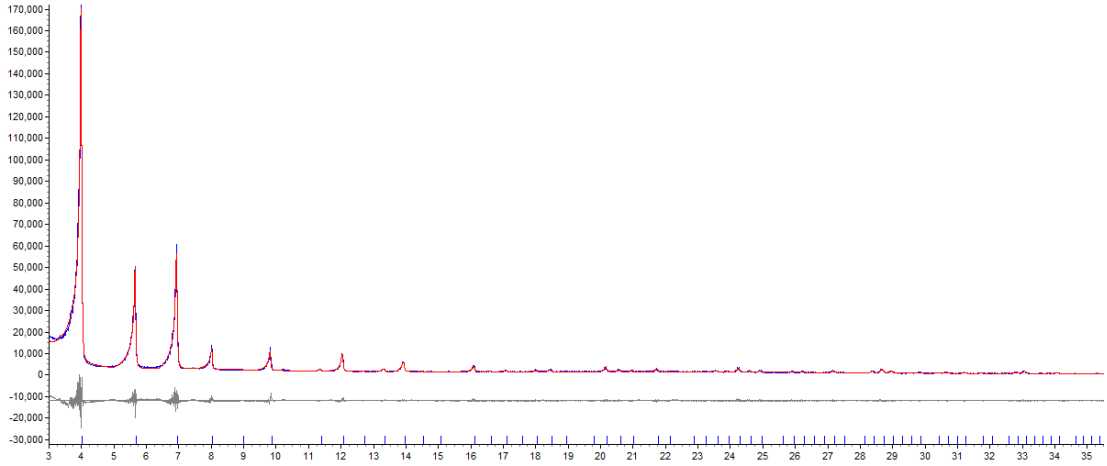

Figure S41. Experimental (blue line), calculated (red line) and difference plot (grey line) for Pawley fitting of the diffraction data obtained for activated **1** in cubic space group Pm$\bar{3}$m with refined values of a/b/c= 21.957(1) Å. The indexed peak positions are shown by the blue tick marks. R_{wp}= 8.85%, R_{exp}= 1.77%, R_p= 7.17%, χ^2= 4.98.

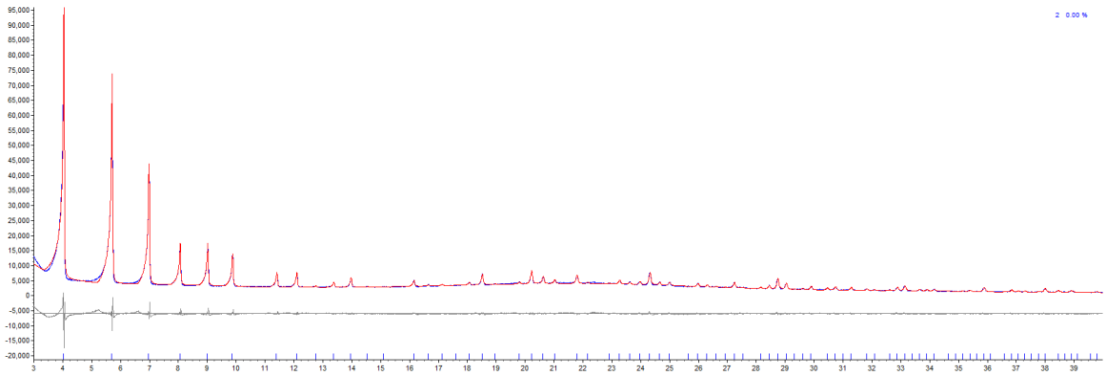

Figure S42. Experimental (blue line), calculated (red line) and difference plot (grey line) for Pawley fitting of the diffraction data obtained for as-made **2** in cubic space group Pm$\bar{3}$m with refined values of a/b/c= 21.961(6) Å. The indexed peak positions are shown by the blue tick marks. R_{wp}= 4.77%, R_{exp}= 1.56%, R_p= 3.47%, χ^2= 3.04.

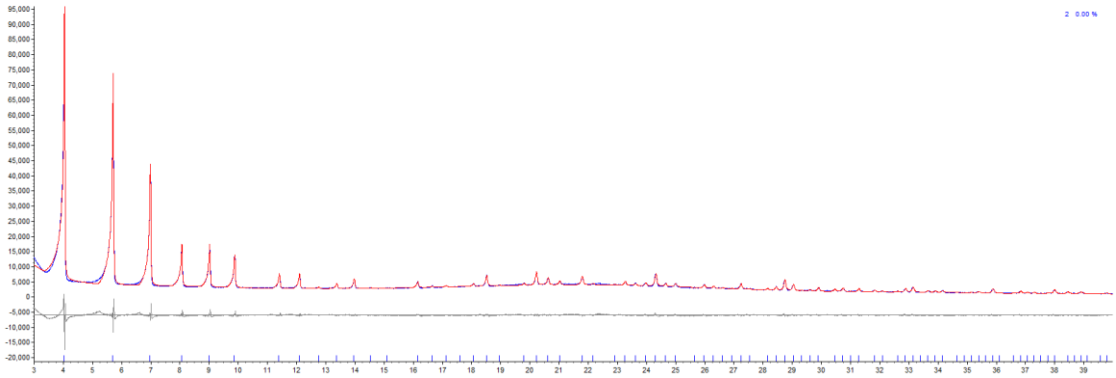

Figure S43. Experimental (blue line), calculated (red line) and difference plot (grey line) for Pawley fitting of the diffraction data obtained for activated **2** in cubic space group Pm$\bar{3}$m with refined values of a/b/c= 21.985(2) Å. The indexed peak positions are shown by the blue tick marks. R_{wp}= 4.73%, R_{exp}= 1.48%, R_p= 3.66%, χ^2= 3.18.

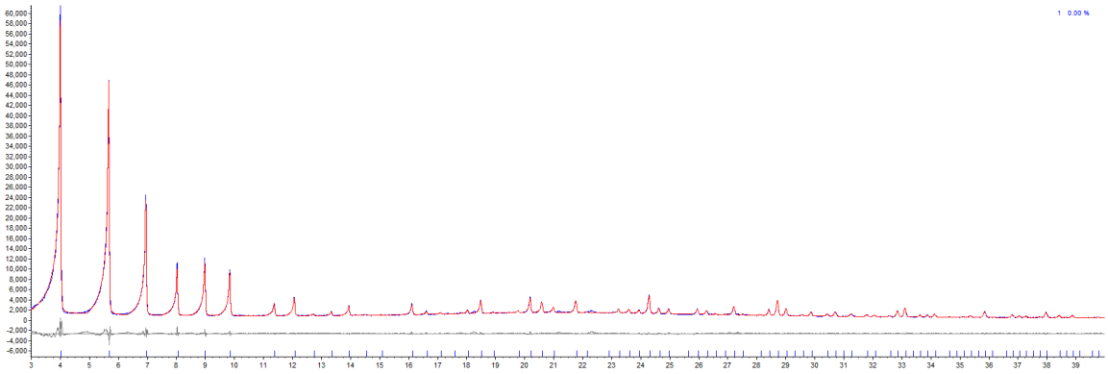

Figure S44. Experimental (blue line), calculated (red line) and difference plot (grey line) for Pawley fitting of the diffraction data obtained for as-made **3A** in cubic space group $Pm\bar{3}m$ with refined values of a/b/c= 21.946(3) Å. The indexed peak positions are shown by the blue tick marks. R_{wp}= 5.23%, R_{exp}= 2.35%, χ^2= 2.2.

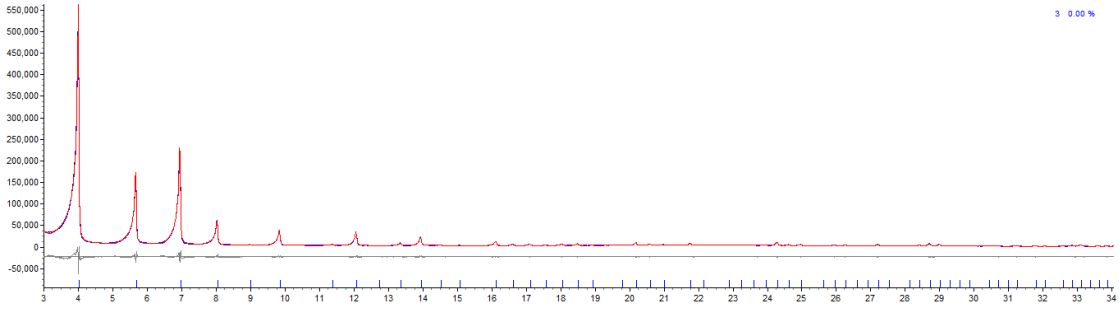

Figure S45. Experimental (blue line), calculated (red line) and difference plot (grey line) for Pawley fitting of the diffraction data obtained for activated **3A** in cubic space group $Pm\bar{3}m$ with refined values of a/b/c= 21.959(1) Å. The indexed peak positions are shown by the blue tick marks. R_{wp}= 5.60%, R_{exp}= 0.98%, R_p= 4.35%, χ^2= 5.71.

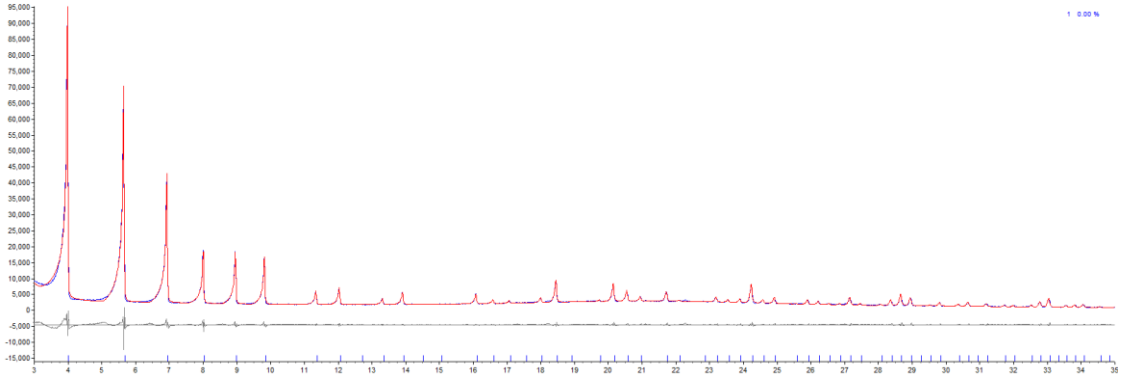

Figure S46. Experimental (blue line), calculated (red line) and difference plot (grey line) for Pawley fitting of the diffraction data obtained for as-made **3B** in cubic space group $Pm\bar{3}m$ with refined values of a/b/c= 21.9821(3) Å. The indexed peak positions are shown by the blue tick marks. R_{wp}= 5.97%, R_{exp}= 1.71%, χ^2= 3.5.

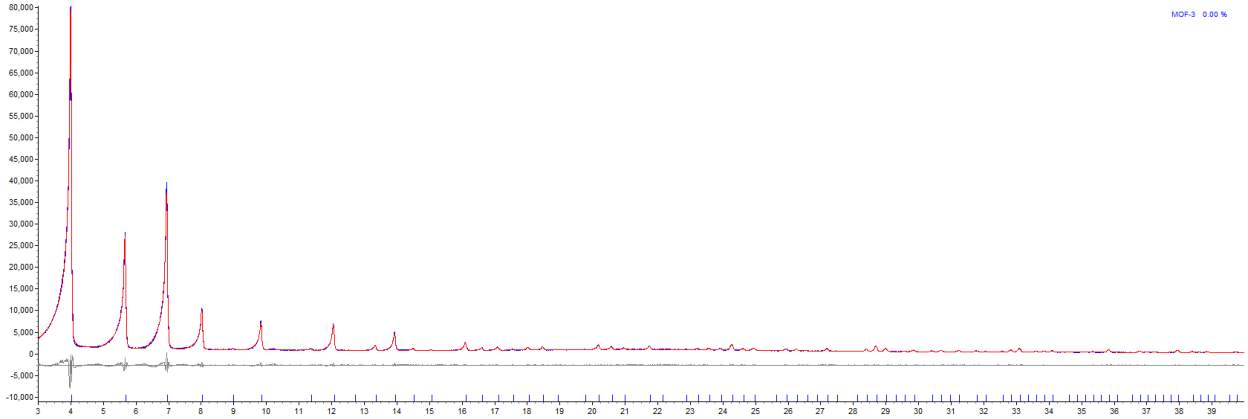

Figure S47. Experimental (blue line), calculated (red line) and difference plot (grey line) for Pawley fitting of the diffraction data obtained for activated **3B** in cubic space group Pm$\bar{3}$m with refined values of a/b/c= 21.9619(5) Å. The indexed peak positions are shown by the blue tick marks. R_{wp}= 5.29%, R_{exp}= 2.41%, χ^2= 2.19.

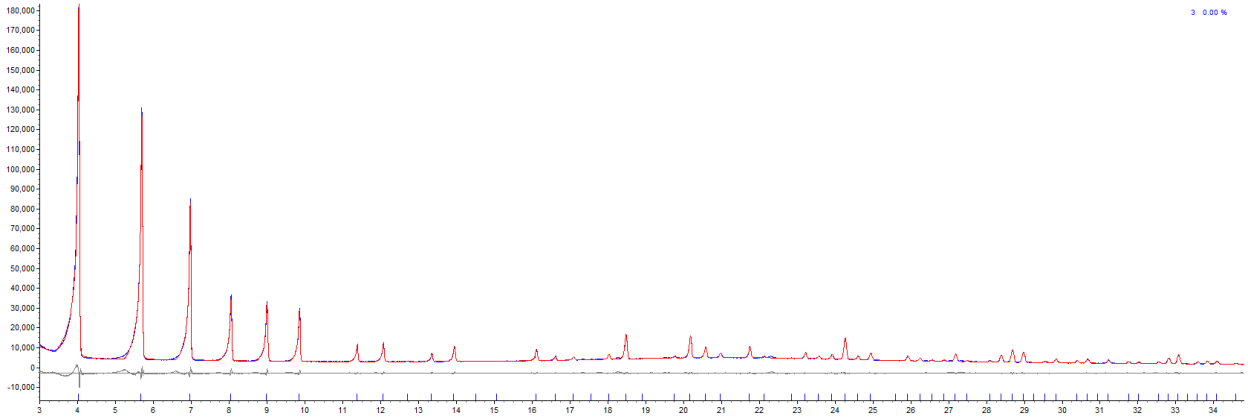

Figure S48. Experimental (blue line), calculated (red line) and difference plot (grey line) for Pawley fitting of the diffraction data obtained for as-made **3C** in cubic space group Pm$\bar{3}$m with refined values of a/b/c= 21.996(1) Å. The indexed peak positions are shown by the blue tick marks. Final R_{wp}= 4.39%, R_{exp}= 1.32%, χ^2= 3.30.

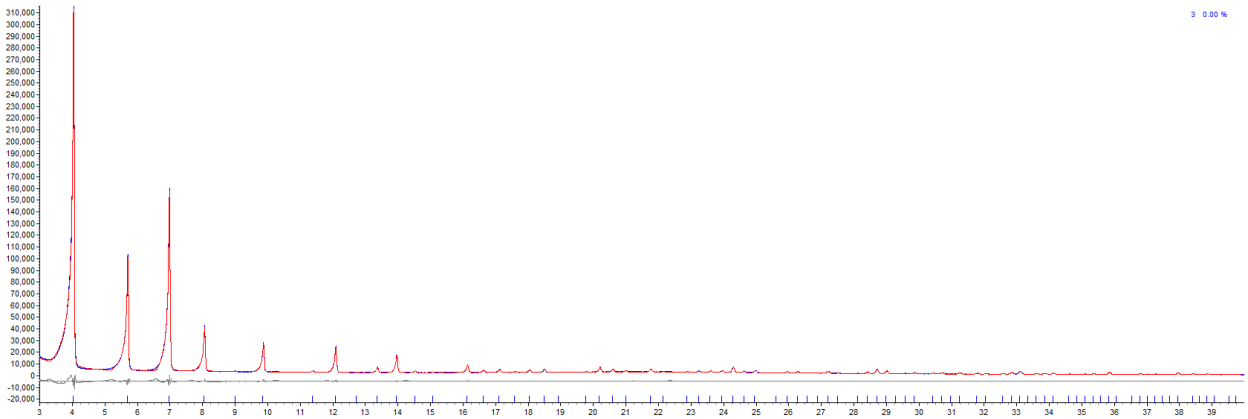

Figure S49. Experimental (blue line), calculated (red line) and difference plot (grey line) for Pawley fitting of the diffraction data obtained for activated **3C** in cubic space group Pm$\bar{3}$m with refined values of a/b/c= 21.98(3) Å. The indexed peak positions are shown by the blue tick marks. Final R_{wp}= 5.31%, R_{exp}= 1.37%, χ^2= 3.89

Table S9. Lattice parameters of **1, 2, 3A, 3B, and 3C** as-made and activated samples from PXRD data

MOF	As-made (Å)	Activated (Å)
1	21.916(1)	21.957(1)
3A	21.946(3)	21.959(1)
3B	21.9821(3)	21.9619(5)
3C	21.996(1)	21.98(3)
2	21.961(6)	21.985(2)

SI 14. Water Stability of MOFs: ICP, XRD, and BET analysis

General procedure: 20 mg of as-made MOF was placed in a vial containing 6 mL of distilled water. The vial was stored at RT or 120 °C for 48 hours. Syringe filters, Acrodisc® GHP, 13 mm, 0.2 μm were used to filter the final solution. The filtrate was analyzed for Zr leaching using the ICP technique.

Table S10: Zr leaching from ICP analysis

Entry	MOF	Solution	T/°C	t/h	Wt%
1	**1**	H_2O_{dist}	rt	48	0.00[a]
2	**2**	H_2O_{dist}	rt	48	1.77×10^{-3}
3	**3A**	H_2O_{dist}	rt	48	0.00 [a]
4	**3B**	H_2O_{dist}	rt	48	0.00 [a]
5	**3C**	H_2O_{dist}	rt	48	0.19×10^{-3}
7	**1**	H_2O_{dist}	120	48	0.04×10^{-3}
8	**2**	H_2O_{dist}	120	48	0.347
9	**3A**	H_2O_{dist}	120	48	0.00 [a]
10	**3B**	H_2O_{dist}	120	48	0.00 [a]
11	**3C**	H_2O_{dist}	120	48	0.25×10^{-3}

[a] Same as background.

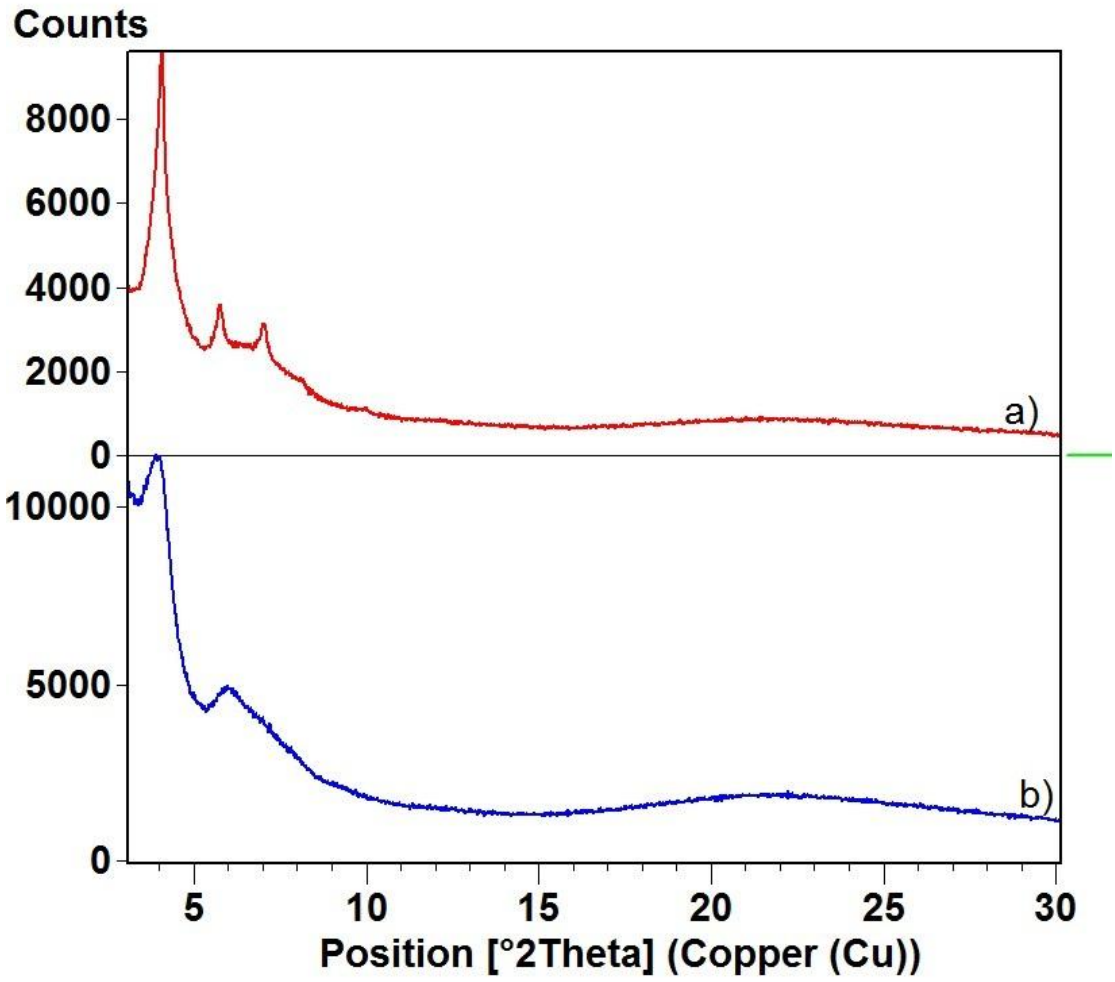

Figure S50. PXRD patterns of **1** after treating with water for 48 h; i) treated at RT and dried under vacuum before analysis; ii) treated at 120 °C and dried under vacuum before analysis. The collapse of structure under vacuum corroborates the poor mechanical stability of **1**. Contrary, activation with supercritical CO_2 yields crystalline material (main text, Figure 2a).

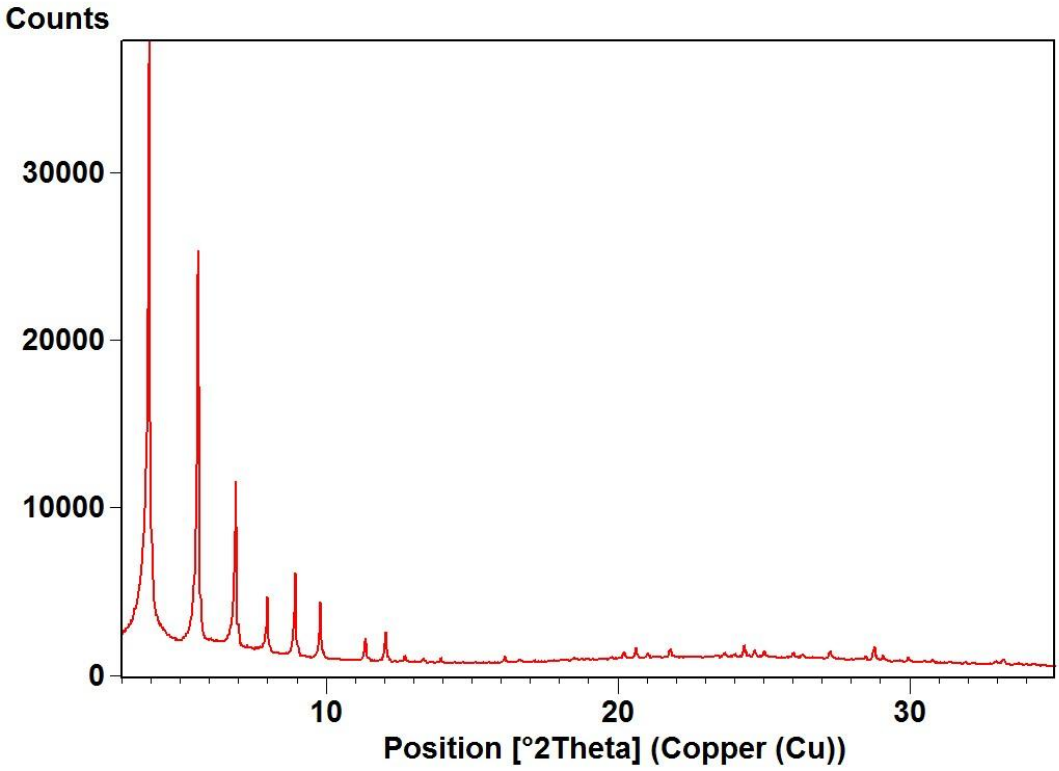

Figure S51. PXRD pattern of **3A** after treatment with water at RT for 48 h. The samples are filtered and dried shortly before analysis.The retention of PXRD pattern confirms that **3A** is both chemically and mechanically stable.

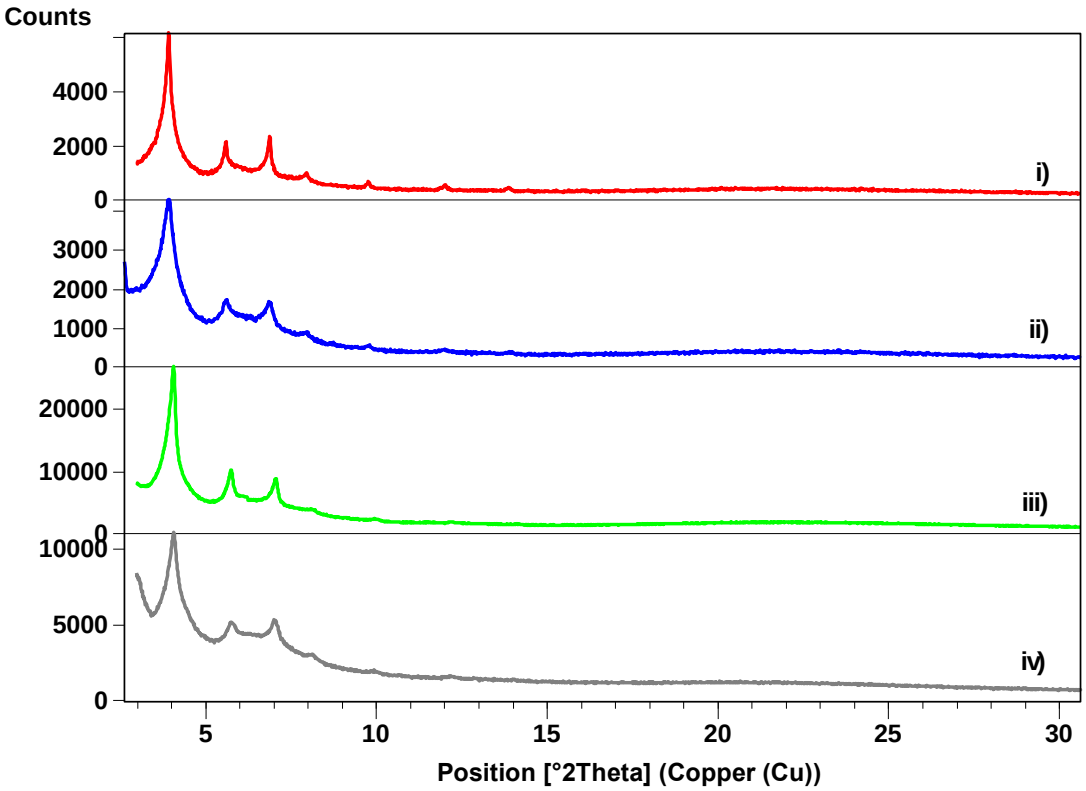

Figure S52. PXRD pattern of i) **3B** after treating with water at RT; ii) **3B** after treating with water at 120 °C; iii) **3C** after treating with water at RT; iv) **3C** after treating with water at 120 °C. The samples are filtered and dried before analysis. The broad reflections indicates that both **3B** and **3C** are not stable in water at RT.

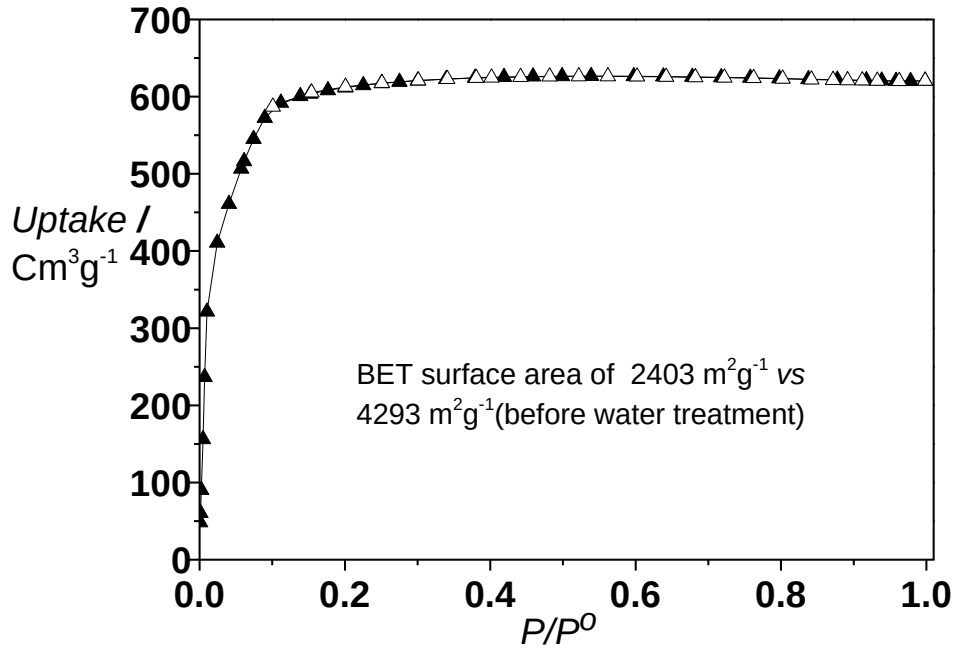

Figure S53. N_2 isotherm of **3B** after water treatment at RT followed by activation. **3B** loses 56 % and 58 % of its initial surface area and pore volume, respectively after treatment with water RT. In sharp contrast, **3A** (with 15 % of ptba) retains all its surface area and pore volume (**Table S11**). This suggests with increase in ptba content in mixed ligand MOFs, the chemical stability decreases.

Table S11. Changes in the BET surface area /pore volume of **1, 2, 3A,** and **3B** before and after water stability test at RT.

MOF [a]	**Pore Volume / cm^3g^{-1}**		**BET surface area/m^2g^{-1}**	
	before	after	before	after
1	1.68	1.57	4,342	4,016
2	1.55	0.00	4,116	45
3A	1.62	1.61	4,120	4,184
3B	1.65	0.96	4,293	2,403

[a] all the powders were filtered and exchanged with ethanol after stability test, and finally activated with super critical CO_2.

SI 15.Solvent assisted ligand exchange[24]

40 mg (0.005mmol) of as-made **1** is loaded into a 40 mL reaction vial containing 12 mL of 1 mM $ptbaH_4$ solution in NMP (0.011mmol). The reaction vial was placed in a preheated oven at 90 °C and maintained at that temperature for 48 h. The color of the crystals changed from light green to light orange. However, repeated washings of crystals after the reaction with DMF solvent rendered initial colour to the crystal. This suggests that ligand exchange did not take place. Further confirmation was obtained from NMR spectroscopy(figure S54). The NMR spectrum after digestion of MOF in DCl/DMSO mixture shows presence of only $bptbaH_4$ in the MOF after reaction.

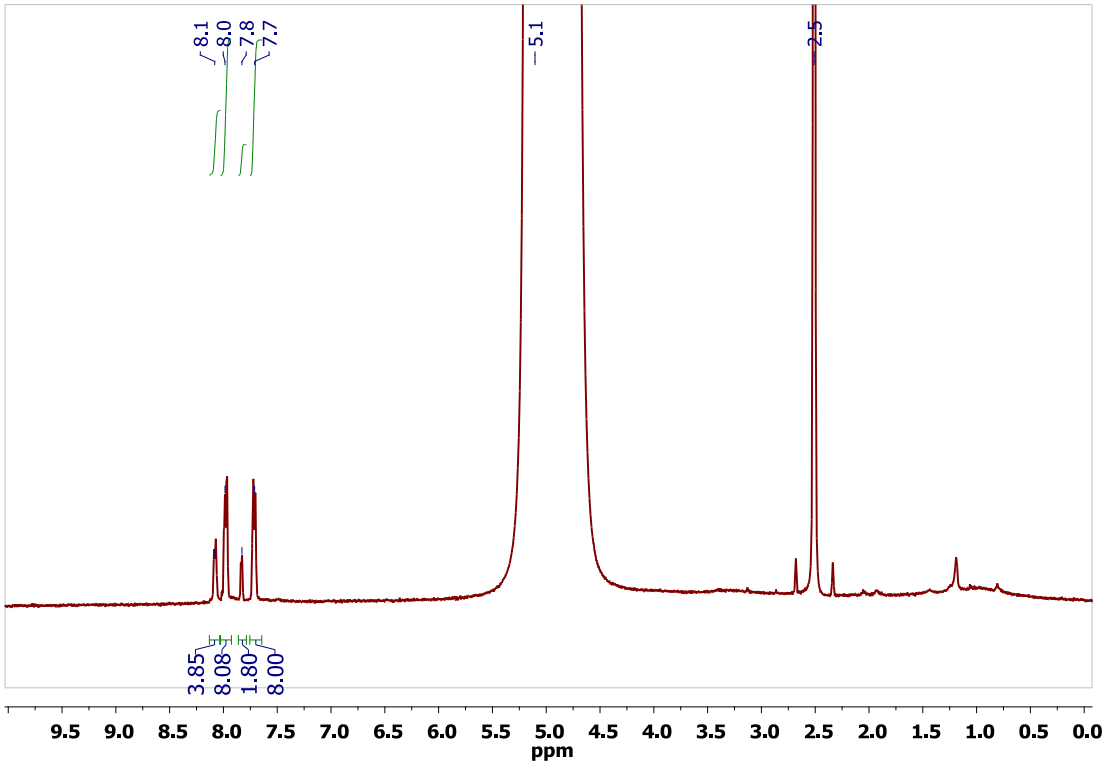

Figure S54. ^{1}H NMR spectrum of **1** in DMSO-d_6 after ligand exchange with $ptbaH_4$. The MOF was digested with 20 wt % DCl.

SI 15. References

1. J. Rouquerol, P. Llewellyn, F. Rouquerol, *Stud. Surf. Sci. Catal.* **2007**, *160*, 49
2. L. Czepirski, J. Jagiello, *Chem. Eng. Sci.* **1989**, *44*, 797
3. A. Myers, *Adsorption* **2003**, *9*, 9.
4 .K. Fujimoto, H. Shimizu, M. Furusyo, S. Akiyama, M. Ishida, U. Furukawa, T.Yokoo, M. Inouye, *Tetrahedron* **2009**, *65*, 9357.
5. A. P. Nelson, O. K. Farha, K. L. Mulfort, J. T. Hupp, *J. Am. Chem. Soc.* **2009**, *131*, 458.
6. a) J. Cavka, S. Jakobsen, U. Olsbye, N. Guillou, C. Lamberti, S. Bordiga, K. Lillerud, *J. Am. Chem. Soc.* **2008**, *130*, 13850–13851; b) L. Valenzano, B. Civalleri, S. Chavan, S. Bordiga, M. H. Nilsen, S. Jakobsen, K. P. Lillerud and C. Lamberti, *Chem. Mater.* **2011**, *23*, 1700–1718

7. T. Düren, L. Sarkisov, R. Q. Snurr, **2007**. For more details see: H. Frost, T. Düren, R. Q. Snurr, *J. Phys. Chem. B* **2006**, *110*, 9565–9570
8. J. E. Warren, *Free My Data (FMD) - an automated frame conversion program utilising Simon Parson's Eclipse and Bruker Frm2Frm executables* **2010**.
9. Bruker, *APEXII 2010* **2010**.
10. Bruker, *SAINT, 7.68A* **2009**.
11. Bruker, *SADABS* **2008**.
12. a) O. V. Dolomanov, L. J. Bourhis, R. J. Gildea, J. A. K. Howard, H. Puschmann, *J. Appl. Crystallogr.* **2009**, *42*, 339; b) L. J. Bourhis, O. V. Dolomanov, R. J. Gildea, J. A. K. Howard, H. Puschmann, *olex2.solve* **2011**.
13. G. Sheldrick, *Acta Crystallographica Section A* **2008**, *64*, 112.
14. Bruker, *XPREP*¸**2004**
15. A. L. Spek, *Acta Cryst*allographica *Section D* **2009**, *65*, 148.
16. I. A. Guzei, *J. Appl. Crystallogr.* **2014**, *47*, 806.
17 .M. D. Hanwell, D. E. Curtis, D. C. Lonie, T. Vandermeersch, E. Zurek, G. R. Hutchison *J. Cheminf.* **2012**, 4:17
18. M. P. Johansson, J. Olsen, *J. Chem. Theory Comput*. **2008**, *4*, 1460.
19. G. Kresse and J. Hafner. *Phys. Rev. B* **1993**, *47*, 558.
20. P. E. Blochl, *Phys. Rev. B* **1994**, *50*, 17953.
21. J. P. Perdew, K. Burke, M. Ernzerhof, *Phys. Rev. Lett.* **1996**, *77*, 3865.
22. M. Dion, H. Rydberg, E. Schröder, D. C. Langreth, B. I. Lundqvist, *Phys. Rev. Lett.* **2004**, *92*, 246401.
23. H. T. Stokes and D. M. Hatch, *J. Appl. Cryst*. **2005**, *38*, 237.
24. O. Karagiaridi, W. Bury, J. E. Mondloch, J. T. Hupp, O. K. Farha *Angew. Chem. Int. Ed.* **2014**, *53*, 4530-4540